SUBMITTED TO ApJ, NOVEMBER 2, 2012
Preprint typeset using LaTeX style emulateapj v. 12/01/06

arXiv:1211.1380v1 [astro-ph.CO] 6 Nov 2012

MAGIICAT II. GENERAL CHARACTERISTICS OF THE MgII ABSORBING CIRCUMGALACTIC MEDIUM

NIKOLE M. NIELSEN[1], CHRISTOPHER W. CHURCHILL[1], AND GLENN G. KACPRZAK[2,3]

Submitted to ApJ, November 2, 2012

ABSTRACT

We fully characterize the MgII absorbing circumgalactic medium (CGM) using the "MgII Absorber-Galaxy Catalog" (MAGIICAT), a compilation comprising 169 intermediate redshift ($0.1 \leq z \leq 1.1$) galaxies within 200 kpc (projected) of background quasars. We examine the rest-frame equivalent widths, $W_r(2796)$, and covering fractions, f_c, down to $W_r(2796) \simeq 0.003$ Å, against galaxy redshift, B- and K-band luminosity, $B-K$ color, and impact parameter, D. We also present B- and K-band luminosity functions for different $W_r(2796)$ and redshift regimes. The radial extent of the MgII absorbing CGM, $R(L) = R_*(L/L^*)^\beta$, exhibits little dependency on $W_r(2796)$ threshold in the B-band, but becomes less sensitive to luminosity in the K-band. In both the B- and K-bands, $R(L)$ has a much steeper luminosity dependence for bluer galaxies than for redder galaxies, and for lower redshift galaxies compared to higher redshift galaxies. The covering fractions exhibit clear differential dependencies on $W_r(2796)$ threshold, galaxy luminosity, and redshift as a function of impact parameter. Lower luminosity galaxies exhibit no MgII absorption beyond 100 kpc, whereas higher luminosity galaxies have $0.1 \leq f_c \leq 0.3$ beyond 100 kpc, with f_c decreasing with increasing $W_r(2796)$ threshold. Redshift evolution is found in the B-band luminosity function for galaxies associated with $W_r(2796) < 0.3$ Å absorption. Many of our findings are in conflict with previously published works. We address these conflicts and discuss the implications of our results for the low-ionization, intermediate redshift CGM.

Subject headings: galaxies: halos — quasars: absorption lines

1. INTRODUCTION

Understanding the formation and evolution of galaxies is one of the foremost problems facing extragalactic research. Over the last decade, theoretical activity has been focused on studying how galaxies form and evolve in the context of the response of baryonic gas to dark matter halos of various masses and to physical processes such as stellar and AGN feedback (e.g., Birnboim & Dekel 2003; Maller & Bullock 2004; Kereš et al. 2005; Dekel & Birnboim 2006; Birnboim et al. 2007; Ocvirk, Pichon, & Teyssier 2008; Kereš et al. 2009; Oppenheimer et al. 2010; Stewart et al. 2011; van de Voort et al. 2011; van de Voort & Schaye 2011). These theoretical works have established that the circumgalactic medium (CGM) is a dynamic environment comprising inflowing accretion, outflowing winds, and gas that recycles between the halo and galaxy.

What has become clear is that the CGM is intimately linked to galaxy morphology, stellar populations and kinematics, and chemical evolution. The detailed physics governing the heating and cooling of baryonic gas regulates the formation and galactic-scale dynamical motions of stars, which in turn feedback and govern the physics of the gas in the CGM (e.g., Dekel & Silk 1986; Ceverino & Klypin 2009). Since this paradigm of galaxy evolution suggests a strong CGM-galaxy connection, many investigators have taken a phenomenological approach to developing models that predict the observable geometric distribution and kinematics of baryonic gas in and around galaxies (e.g., Weisheit 1978; Lanzetta & Bowen 1992; Charlton & Churchill 1996; Mo & Miralda-Escude 1996; Benjamin & Danly 1997; Charlton & Churchill 1998; Tinker & Chen 2008; Chelouche & Bowen 2010; Bouché et al. 2011).

As such, the CGM is an astrophysical environment which, at any point in the evolution of a galaxy, yields clues to both its historical development and future evolution. Therefore, observations of the CGM around individual galaxies promise to provide highly sought constraints on the physics governing the global properties of galaxies. In practice, the CGM is almost exclusively accessible via absorption lines present in the spectra of background objects (traditionally using the technique of quasar absorption lines). Studying the CGM-galaxy connection is desirable over all redshifts, however, the vast majority of work to date has been focused on $z \leq 1$ (however, cf., Adelberger et al. 2005; Simcoe et al. 2006; Steidel et al. 2010), where galaxy photometric and spectral properties can be measured with relatively high accuracy and modest investment in telescope time.

Campaigns to study the CGM in absorption at $z \leq 1$ have targeted OVI absorption (e.g., Tumlinson et al. 2011), CIV absorption (e.g., Chen et al. 2001a), and neutral hydrogen Lyα absorption (e.g., Lanzetta et al. 1995; Chen et al. 2001b). However, by far the vast majority of surveys have focused on MgII absorption (Bergeron & Boissè 1991; Bechtold & Ellingson 1992; Yanny & York 1992; Le Brun et al. 1993; Steidel, Dickinson, & Persson 1994; Steidel 1995; Churchill et al. 1996; Steidel et al. 1997; Guillemin & Bergeron 1997; Churchill et al. 2000b, 2005; Tripp & Bowen 2005; Churchill et al. 2007; Chen & Tinker 2008; Kacprzak et al. 2008; Barton & Cooke 2009; Chen et al. 2010a; Kacprzak, Murphy, & Churchill 2010; Kacprzak et al. 2011a,b; Churchill et al. 2012a).

The MgII $\lambda\lambda 2796, 2803$ doublet is especially well suited at intermediate redshifts since the absorption is observable in the optical. Furthermore, MgII absorption is ideal for tracing low ionization, metal-enriched CGM gas in that it arises in a wide

---

[1] New Mexico State University, Las Cruces, NM 88003 `nnielsen@nmsu.edu, cwc@nmsu.edu`
[2] Swinburne University of Technology, Victoria 3122, Australia `gkacprzak@astro.swin.edu.au`
[3] Australian Research Council Super Science Fellow

range of H I environments, from $\log N(\text{H I}) \simeq 16.5$ to greater than 21.5 (Bergeron & Stasińska 1986; Steidel & Sargent 1992; Churchill et al. 1999, 2000a; Rao & Turnshek 2000; Rigby, Charlton, & Churchill 2002). It is also well established that Mg II absorption probes key CGM structures such as outflow gas (Tremonti et al. 2007; Weiner et al. 2009; Martin & Bouché 2009; Rubin et al. 2010) and inflow gas (Ribaudo et al. 2011; Rubin et al. 2011; Thom et al. 2011; Kacprzak et al. 2012) associated with galaxies.

Through the efforts of the aforementioned studies, the behavior of Mg II CGM absorption in relation to various galaxy properties has been incrementally characterized over the last two decades. Examples of some of the findings include relationships between the strength of Mg II absorption and galaxy luminosity (Kacprzak et al. 2008; Chen et al. 2010a), galaxy mass (Bouché et al. 2006; Gauthier et al. 2009; Churchill et al. 2012b), star formation or specific star formation rate (Chen et al. 2010b; Ménard et al. 2011), galaxy color (Zibetti et al. 2007; Bordoloi et al. 2011), galaxy morphology (Kacprzak et al. 2007), and galaxy orientation (Bordoloi et al. 2011; Bouché et al. 2011; Kacprzak et al. 2011b; Kacprzak, Churchill, & Nielsen 2012; Churchill et al. 2012a).

Generally speaking, these investigations have yielded results that appear to be converging on an observational portrait of the Mg II absorbing CGM that is more or less consistent with the broad scenario forwarded by theory and simulations. For example, evidence is mounting that accretion may preferentially reside in a coplanar geometry (e.g., Steidel et al. 1997; Kacprzak et al. 2010; Stewart et al. 2011; Kacprzak et al. 2011b), whereas winds may outflow along the galaxy minor axis (Bordoloi et al. 2011; Bouché et al. 2011; Churchill et al. 2012a; Kacprzak, Churchill, & Nielsen 2012). However, due to the complex ionization structure, non-uniform metal enrichment, and dynamical processes of the CGM, and due to the wide range of galaxy properties, such as luminosity, color, mass, and morphology, the data exhibit substantial scatter. As such, while some works have found statistically significant correlations between two quantities or between combined/scaled quantities, many works have reported connections between galaxy and Mg II absorption CGM properties either based on general trends (i.e., correlations that are not statistically significant above the 3 σ level) or on slight reductions in the scatter of certain relationships by combining/scaling one or more measured quantity.

Motivated by the potential that combining the data from our work and other surveys may further illuminate the CGM-galaxy connection, we have endeavored to assemble a database of the extant works focused on Mg II absorption from the CGM of intermediate redshift galaxies. We also aim to provide a large uniform data set based upon a single cosmological parameter set and to consolidate the measurements of given galaxy-absorber pairs duplicated in various works. Such a compilation holds the promise of yielding higher statistical significance in the already published results, and of providing greater leverage for exploring the dependence of CGM Mg II absorption with, for example, redshift, galaxy luminosity/color, or impact parameter as a function of equivalent width threshold.

The data and full details of the "Mg II Absorber-Galaxy Catalog" (MAGIICAT) we have compiled, which we briefly describe in § 2, will be presented in Paper I of this series (Nielsen et al. 2013). In this paper, we utilize the data to address several long-standing questions with regard to the Mg II CGM-galaxy connection. In § 2, we briefly describe the galaxy sample, which has uniform photometric properties and impact parameters for a ΛCDM cosmology ($H_0 = 70$ km s^{-1} Mpc^{-1}, $\Omega_M = 0.3$ and $\Omega_\Lambda = 0.7$). In § 3, we present an examination of (1) galaxy color and absolute magnitude evolution, (2) the dependence of $W_r(2796)$ on galaxy color, (3) the dependence of $W_r(2796)$ on impact parameter, (4) covering fraction as a function of impact parameter and $W_r(2796)$ for luminosity, color, and redshift subsamples, (5) the luminosity scaling of "halo absorption radius" and the behavior of covering fraction with $W_r(2796)$, galaxy color, and redshift, and (6) B- and K-band luminosity functions. In § 4, we discuss the implications of our results and give concluding remarks in § 5.

2. GALAXY SAMPLE AND SUBSAMPLES

From an exhaustive literature search, we compiled a catalog of galaxies with spectroscopic redshifts $0.1 \leq z \leq 1$ within a projected distance of $D \leq 200$ kpc from a background quasar, regardless of known Mg II absorption. We did not include galaxies for which $W_r(2796)$ measurements could not be obtained. We also distinguish between isolated and group galaxies, where group galaxies have a nearest neighbor within 100 kpc and have a velocity separation no greater than 500 km s^{-1}. The total catalog consists of 205 galaxies. Full details of all galaxies and Mg II absorption properties will be presented in Paper I. Here we briefly describe the general properties of MAGIICAT.

The sample presented here comprises 169 isolated galaxies toward 117 sightlines, covering a redshift range $0.072 \leq z_{\text{gal}} \leq 1.120$, with a median of $\langle z \rangle = 0.346$. The impact parameter range is $5.5 \leq D \leq 193$ kpc, with median $\langle D \rangle = 48$ kpc.

For each galaxy, we determined rest-frame AB absolute magnitudes, M_B and M_K, by computing k-corrections appropriate for the observed magnitudes (e.g., Kim, Goobar, & Perlmutter 1996) using the extended Coleman et al. (1980) spectral energy distribution (SED) templates from Bolzonella et al. (2000). We selected a galaxy SED by comparing the observed galaxy colors to the redshifted SEDs. Luminosities, L_B/L_B^* and L_K/L_K^*, were obtained using a linear fit to M_B^* with redshift from Faber et al. (2007) (B-band) and using $M_K^*(z)$ as expressed in Eq. 2 from Cirasuolo et al. (2010) (K-band). Absolute B-band magnitudes range from $-16.1 \geq M_B \geq -22.8$, corresponding to luminosities of $0.017 \leq L_B/L_B^* \leq 7.44$, with median $L_B/L_B^* = 0.526$. Absolute K-band magnitudes range from $-17.0 \geq M_K \geq -24.3$, corresponding to $0.006 \leq L_K/L_K^* \leq 4.9$. Rest-frame $B-K$ colors range from $0.04 \leq B-K \leq 4.09$, with median $B-K = 1.39$. We obtain $B-K$ colors for all but 21 of the galaxies.

MAGIICAT was bifurcated into several subsamples for analysis. When dividing the galaxy-absorber pairs into subsamples, we either take a sample driven approach by splitting the sample at the median value of a given observed quantity, or dividing the sample based upon historical precedent, such as $W_r(2796)$ cuts. The full sample was bifurcated based on the median galaxy redshift, L_B/L_B^*, L_K/L_K^*, or $B-K$. Table 1 presents the characteristics of the full sample and each subsample, including the number of galaxies, the median value by which the catalog was cut, and the minimum, maximum, and mean values of galaxy redshift, B- and K-band luminosity, and $B-K$ color. The subsample names listed will be used throughout this paper.

TABLE 1
SUBSAMPLE CHARACTERISTICS

			$z_{\rm gal}$			L_B/L_B^*			L_K/L_K^*			$B-K$		
Subsample	# Gals	Cut[a]	Min	Max	Mean	Min	Max	Mean	Min[b]	Max[b]	Mean[b]	Min[b]	Max[b]	Mean[b]
All	169	···	0.072	1.120	0.415	0.017	7.441	0.780	0.006	4.901	0.653	0.038	4.090	1.471
Low z	84	0.346	0.072	0.340	0.222	0.017	7.441	0.740	0.006	4.901	0.621	0.430	3.042	1.571
High z	85	0.346	0.346	1.120	0.606	0.071	4.801	0.820	0.016	3.152	0.685	0.038	4.090	1.370
Low L_B/L_B^*	84	0.526	0.072	0.941	0.395	0.017	0.523	0.276	0.006	1.680	0.266	0.038	4.090	1.446
High L_B/L_B^*	85	0.526	0.096	1.120	0.436	0.526	7.441	1.278	0.214	4.901	1.020	0.483	2.537	1.494
Low L_K/L_K^*	74	0.414	0.110	0.941	0.386	0.019	1.214	0.324	0.006	0.406	0.193	0.038	3.037	1.230
High L_K/L_K^*	74	0.414	0.096	1.017	0.419	0.189	7.441	1.231	0.423	4.901	1.114	0.483	4.090	1.711
Blue	74	1.391	0.098	1.017	0.443	0.019	7.441	0.844	0.006	2.985	0.443	0.038	1.384	0.996
Red	74	1.391	0.096	0.852	0.362	0.035	3.759	0.711	0.026	4.901	0.864	1.399	4.090	1.945

[a] The median value by which each subsample was bifurcated. The cut is inclusive to the "high" and red bins.
[b] Only including galaxies with a value for M_K.

3. RESULTS

In this section, we report on the luminous properties of the galaxies and directly compare them to the properties of the Mg II absorbing CGM. The analysis presented here is based upon direct observables. We do not scale or combine measured quantities. We also do not scale or fit the data to models of the CGM. Our aim is to characterize the Mg II CGM-galaxy connection directly with no assumptions and to provide information that can be directly interpreted in terms of primary observables. We examine only bivariate relationships, reserving further analysis, such as multivariate techniques for future work to appear in later papers of this series.

3.1. *Galaxy Redshifts, Colors, and Magnitudes*

Since the CGM as probed by Mg II may depend upon galaxy stellar populations, and these populations are known to evolve, we examined whether the galaxy rest-frame colors and magnitudes evolve with redshift for the sample. A Kendall-τ rank correlation test on $B-K$ versus $z_{\rm gal}$ shows that the null hypothesis of no correlation can be ruled out to a confidence level (CL) no better than 2.3 σ[4]. A rank correlation test yielded a 4.4 σ significance that M_B correlates with $z_{\rm gal}$, whereas M_K is consistent with no evolution (2.1 σ).

Faber et al. (2007) found that M_B^* brightens with increasing redshift from the DEEP2+COMBO-17 surveys. The average M_B of the sample presented here increases with redshift more rapidly than M_B^*. Similarly, Cirasuolo et al. (2010) found that M_K^* tends to brighten with increasing redshift from UKIDSS, whereas the average M_K of the sample presented here does not appear to evolve. As such, we may be seeing that galaxies selected by Mg II absorption are characterized by bluer colors at higher redshift. However, selection effects may be important. Virtually all the galaxies were selected or discovered using the red band in the observer frame, which probes further toward the B-band in the galaxy rest frame with increasing redshift. However, this cannot explain the lack of evolution in the K-band.

Using statistical methods in which individual galaxies were not directly identified with absorbers, Zibetti et al. (2007) reported no color evolution for $0.4 \leq z \leq 1$ using observed g, r, i, and z band magnitudes for $W_r(2796) \geq 0.8$ Å. A direct comparison is difficult because we use optical B-band and 2.2μm infrared absolute magnitudes to determine rest-frame colors and we study systems with much smaller $W_r(2796)$ than represented by their sample. However, bifurcating the sample presented here at $W_r(2796) = 0.8$ Å, we obtain 0.8 σ for $W_r(2796) \geq 0.8$ Å. For $W_r(2796) < 0.8$ Å we obtain 2.5 σ indicating that the systems below the sensitivity of Zibetti et al. (2007) dominate a possible color evolution.

3.2. *$W_r(2796)$, Galaxy Luminosity, and Colors*

To see whether $W_r(2796)$ exhibits some dependency on galaxy luminosity, we performed a non-parametric Kendall's τ rank correlation test that allows for upper limits on either the dependent or independent variable for bivariate data (see Brown, Hollander, & Korwar 1974; Wang & Wells 2000) with $W_r(2796)$ as the dependent variable. The null hypothesis of no correlation could not be ruled out for $W_r(2796)$ against L_B/L_B^* (0.8 σ), L_K/L_K^* (0.2 σ), M_B (1.6 σ), and M_K (0.02 σ). The lack of correlations found here are interesting in view of the compelling arguments by Bouché et al. (2006), who derive an anti-correlation between $W_r(2796)$ and galaxy luminosity with a dependence on the faint-end slope of the galaxy luminosity function and a proportionality between galaxy luminosity and the cross-section of the absorbing CGM.

To determine if $W_r(2796)$ has any dependency on galaxy color, we performed the non-parametric Kendall's τ rank correlation test on $W_r(2796)$ against $B-K$. The test indicates that $W_r(2796)$ does not directly correlate with galaxy color for the full sample (1.1 σ). A Kendall's τ rank correlation test between $W_r(2796)$ and $B-K$ for the subsample with $D \leq 50$ kpc indicates that $W_r(2796)$ is not correlated with color at smaller impact parameters (0.3 σ).

The lack of a correlation between $W_r(2796)$ and $B-K$ is consistent with the findings of Chen et al. (2010a), who examined $B-R$ colors for $0.1 \leq z \leq 0.5$. However, the result is contrary to the statistically based results of Zibetti et al. (2007), who find bluer colors from the integrated light selected by stronger Mg II absorbers and redder colors selected by weaker absorbers for $0.4 \leq z \leq 1$, where the minimum $W_r(2796)$ of their sample is 0.8 Å. A direct comparison with the work of Zibetti et al. (2007) is difficult due to its statistical nature. However, a Kendall's τ test examining the $W_r(2796) \geq 0.8$ Å subsample of MAGIICAT yielded no correlation between $W_r(2796)$ and $B-K$ (1.9 σ).

Bifurcating the full galaxy sample at $W_{\rm cut}$ = 0.1, 0.3, 0.6, and 1.0 Å, we find a 3.1 σ significance for a correlation between $W_r(2796)$ and $B-K$ for galaxies hosting $W_r(2796) \geq$

---

[4] Running the test on $B-R$ versus $z_{\rm gal}$ gives a less significant result (1.9 σ)

1.0 Å absorption; for the very strongest absorbers, the redder the galaxy, the greater the Mg II equivalent width. As mentioned, this is contrary to the findings of Zibetti et al. (2007).

To examine the possible $W_r(2796)$ equivalent width distribution dependence on $B-K$ color, we also performed a Kolmogorov-Smirnov (KS) test comparing the cumulative $W_r(2796)$ distribution functions of red ($B-K \geq 1.39$) and blue ($B-K < 1.39$) galaxies. We limited the test to only include those galaxies with detected Mg II absorption. The two subsamples are statistically consistent with having been drawn from the same parent distribution ($\simeq 0.5\ \sigma$). Limiting the sample to galaxies with $D \leq 50$ kpc, the KS test results remain below 1 σ. Though the distribution for red galaxies has power beyond the largest and smallest $W_r(2796)$ of the blue galaxies, the statistics do not ferret out a difference between the two galaxy subsamples; the average and maximum $W_r(2796)$ for $D \leq 50$ kpc associated with red galaxies and blue galaxies are consistent (average 0.97 and 0.91 Å, with maximum 2.9 and 2.1 Å, respectively).

Our findings that the $W_r(2796)$ distributions from the CGM within $D = 50$ kpc of blue and red galaxies are indistinguishable is at odds with the dramatic finding of Bordoloi et al. (2011), who report a factor of eight larger equivalent width associated blue galaxies compared to red galaxies in stacked spectra for which the CGM is probed within $D = 50$ kpc.

3.3. *$W_r(2796)$ and Impact Parameter*

A commonly known property of Mg II galaxies is the anti-correlation between $W_r(2796)$ and impact parameter, D, (e.g., Lanzetta & Bowen 1990; Bergeron & Boissè 1991; Steidel 1995; Bouché et al. 2006; Kacprzak et al. 2008; Chen et al. 2010a; Churchill et al. 2012a). In Figure 1, we present $W_r(2796)$ versus D. Galaxies with detected Mg II absorption are plotted as red points and those with upper limits on absorption are plotted as blue points with downward arrows.

We performed a non-parametric Kendall's τ rank correlation test on $W_r(2796)$ against D, allowing for upper limits on $W_r(2796)$. For this sample, $W_r(2796)$ is anti-correlated with D at the 8.2 σ level. Since $W_r(2796)$ correlates with the number of clouds (Voigt profile components, Petitjean & Bergeron 1990; Churchill et al. 2003; Evans 2011), this result indicates that either the column densities, velocity spreads, or both, diminish with projected distance from the galaxy.

To parameterize the general behavior of the anti-correlation, we used the Expectation-Maximization maximum-likelihood method (Wolynetz 1979) accounting for upper limits on $W_r(2796)$ to fit a power law (see Chen et al. 2010a), $\log W_r(2796) = \alpha_1 \log D + \alpha_2$, and a log-linear fit (see Churchill et al. 2012a), $\log W_r(2796) = \alpha_1 D + \alpha_2$, to the data. The data are poorly described by a power law due to the substantial population of $W_r(2796) < 0.1$ Å absorbers and upper limits. We present the log-linear fit and its 1 σ uncertainties in Figure 1 for $\alpha_1 = -0.019 \pm 0.002$ and $\alpha_2 = 0.28 \pm 0.11$.

The considerable scatter about this relation *may* suggest that $W_r(2796)$ is governed by physical processes related to the galaxy such as luminosity (cf., Kacprzak et al. 2008; Chen et al. 2010a), mass (cf., Bouché et al. 2006; Gauthier et al. 2009; Churchill et al. 2012b), star formation (cf., Chen et al. 2010b; Ménard et al. 2011), or orientation (cf., Bordoloi et al. 2011; Bouché et al. 2011; Kacprzak et al. 2011b; Kacprzak, Churchill, & Nielsen 2012; Churchill et al. 2012a). Alternatively, the CGM is inherently patchy (Churchill et al. 2007, 2012a).

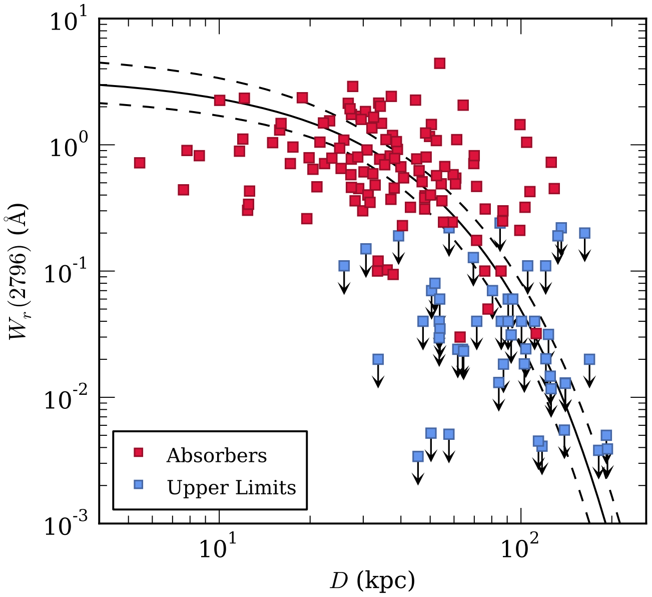

FIG. 1.— The Mg II $\lambda2796$ rest-frame equivalent width, $W_r(2796)$, versus impact parameter, D. Galaxies with detected Mg II absorption are presented as red points, whereas those with upper limits on absorption are blue points with downward arrows. The full sample comprises 169 galaxies with an 8.2 σ anti-correlation between $W_r(2796)$ and D. The solid line is a log-linear maximum likelihood fit to the data, $\log W_r(2796) = \alpha_1 D + \alpha_2$, where $\alpha_1 = -0.019 \pm 0.002$ and $\alpha_2 = 0.28 \pm 0.11$. Dashed curves provide 1 σ uncertainties.

To examine possible trends and/or sources of this scatter in the distribution of $W_r(2796)$ versus D, we applied the two-dimensional Kolmogorov-Smirnov (2DKS) test. This test examines if the 2D distribution of $W_r(2796)$ and D from two samples can be ruled out as being consistent.

We first investigated bifurcations of the full sample about the median values of $B-K$, $z_{\rm gal}$, L_B/L_B^*, and L_K/L_K^*, performing a 2DKS test on the subsamples. Blue galaxies predominantly populate the region $W_r(2796) > 0.3$ Å and $D < 40$ kpc, whereas red galaxies populate the W_r–D plane more uniformly; however, the trend is not statistically significant (1.7 σ). Using a redshift cut, the data show a weak trend for larger $W_r(2796)$ at fixed D for high z galaxies (2.3 σ). A 2DKS test on the luminosities shows that high L_B/L_B^* and L_K/L_K^* are found with larger $W_r(2796)$ at fixed D than low luminosities at the 3.1 σ and 3.3 σ level, respectively.

We also divided the sample into quartiles by L_B/L_B^*, L_K/L_K^*, $B-K$, and $z_{\rm gal}$ and performed the 2DKS test on the lowest and highest quartiles. We obtained $P({\rm KS}) = 0.012$, 0.019, 0.36, and 0.36, for L_B/L_B^*, L_K/L_K^*, $B-K$, and $z_{\rm gal}$, respectively. At best, there is a 2.5 σ correlation that the distribution or scatter of $W_r(2796)$ versus D has a connection to L_B/L_B^*, and a 2.35 σ correlation it is connected to L_K/L_K^*. There is clearly no color or redshift dependence.

3.4. *Covering Fraction and Impact Parameter*

Here we examined the dependence of covering fraction directly on impact parameter and galaxy luminosity, color, and redshift. We present directly observable quantities, making no assumptions with regard to the Mg II absorbing CGM density profile or geometry.

3.4.1. *Covering Fraction Within Fixed Impact Parameters*

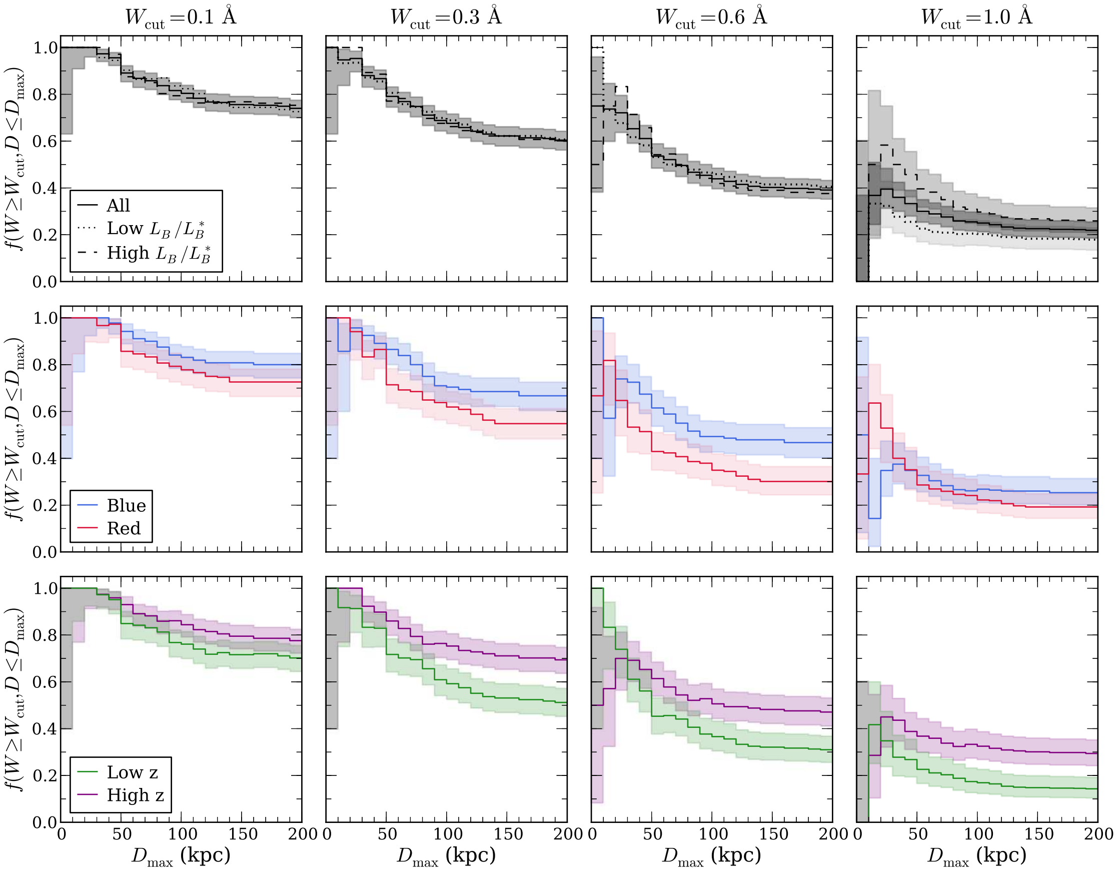

FIG. 2.— The covering fraction, $f_{D\rm max}$, inside $D_{\rm max}$ for different $W_r(2796)$ bifurcations at $W_{\rm cut}$. Shaded regions represent 1 σ uncertainties based upon binomial statistics. — (upper) The full sample of galaxies (solid line), the high luminosity galaxies (dashed line), and the low luminosity galaxies (dotted line), divided at the median B-band luminosity, L_B/L_B^* = 0.526. — (middle) The blue ($B-K < 1.39$) and red ($B-K \geq 1.39$) galaxy subsamples bifurcated at the median galaxy color. — (lower) The high ($z \geq \langle z\rangle$) and low ($z < \langle z\rangle$) redshift galaxy subsamples where $\langle z\rangle$ = 0.346.

In order to examine the covering fraction within a fixed projected radial distance from the galaxies, we computed the quantity $f_{D\rm max} \equiv f(W \geq W_{\rm cut}, D \leq D_{\rm max})$, which we define as the fraction of absorbers with $W_r(2796) \geq W_{\rm cut}$ inside a projected separation of $D_{\rm max}$ from the galaxy.

In Figure 2, we plot $f_{D\rm max}$ against $D_{\rm max}$ in 10 kpc intervals. The uncertainties in $f_{D\rm max}$ are shown as shaded regions. These are the upper and lower limits on $f_{D\rm max}$, calculated using the formalism for binomial statistics (see Gehrels 1986). Values of $f_{D\rm max}$ at $D_{\rm max} \leq 10$ kpc are not robust given the small number of galaxies within this impact parameter[5]. Due to the relative undersampling of galaxies at $D_{\rm max} > 150$ kpc and the cumulative nature of $f_{D\rm max}$, the covering fraction will be virtually unchanging outside this impact parameter; thus the shape of $f_{D\rm max}$ versus $D_{\rm max}$ is less robust for $D_{\rm max} > 150$ kpc.

In Figure 2 (upper panels), we present $f_{D\rm max}$ for the full galaxy sample and for low and high luminosity galaxies. For each $W_{\rm cut}$ subsample, the covering fraction of the Mg II absorbing CGM inside $D = D_{\rm max}$ decreases as $D_{\rm max}$ is increased. At a given $D_{\rm max}$, there is a clear trend that as $W_{\rm cut}$ is increased, $f_{D\rm max}$ decreases, indicating that the covering fraction within a fixed projected separation increases as the minimum absorption threshold is lowered. The covering fraction exhibits no luminosity dependence for $W_{\rm cut}$ = 0.1, 0.3, and 0.6 Å. However, for $W_{\rm cut}$ = 1.0 Å, $f_{D\rm max}$ is larger for high luminosity galaxies at all $D_{\rm max}$ than for low luminosity galaxies. This difference is accentuated at $D_{\rm max} \leq 50$ kpc.

In the middle panels of Figure 2, we present $f_{D\rm max}$ and its uncertainties versus $D_{\rm max}$ for red and blue galaxies. The mean redshift for red galaxies is $\bar{z}$ = 0.36 over the range $0.1 \leq z \leq 0.85$, and for blue galaxies $\bar{z}$ = 0.44 over $0.1 \leq z \leq 1.02$. For each $W_{\rm cut}$ subsample, the blue galaxies have higher covering fractions relative to red galaxies for $D_{\rm max} > 50$ kpc. Within 50 kpc, the larger uncertainties make it difficult to distinguish any possible differences.

In Figure 2 (lower panels), we present $f_{D\rm max}$ and its uncertainties against $D_{\rm max}$ for the high z and low z galaxy subsamples. For $D_{\rm max} \leq 50$ kpc, it is difficult to distinguish any redshift evolution in $f_{D\rm max}$ due to the uncertainties. Beyond 50 kpc, the data suggest that $f_{D\rm max}$ may evolve such that at higher redshift, the covering fraction of Mg II absorbing gas is higher than at lower redshift. The differences in redshift may be connected to the fact that a larger proportion of galaxies at $z \geq \langle z\rangle$ have brighter M_B (see § 3.1).

Chen et al. (2010a) also examined the luminosity dependence of $f_{D\rm max}$ as a function of $W_{\rm cut}$, where their $D_{\rm max}$ is fixed at the luminosity scaled "gas radius", with $R_{\rm gas} \propto (L_B/L_B^*)^{0.35}$, assuming isothermal density profile (Tinker & Chen 2008) and NFW profile (Navarro et al. 1996) models. As such, a direct comparison with our non-parameterized results is difficult. Nonetheless, they found that $f_{D\rm max}$ has little to no depen-

---

[5] Of the three galaxies at $D \leq 10$ kpc, one is at low redshift where the angular separation from the quasar is much greater than the quasar seeing disk, and the other two were found at higher redshift following point spread function subtraction of the quasar (Steidel, Dickinson, & Persson 1994), which was not performed in all surveys.

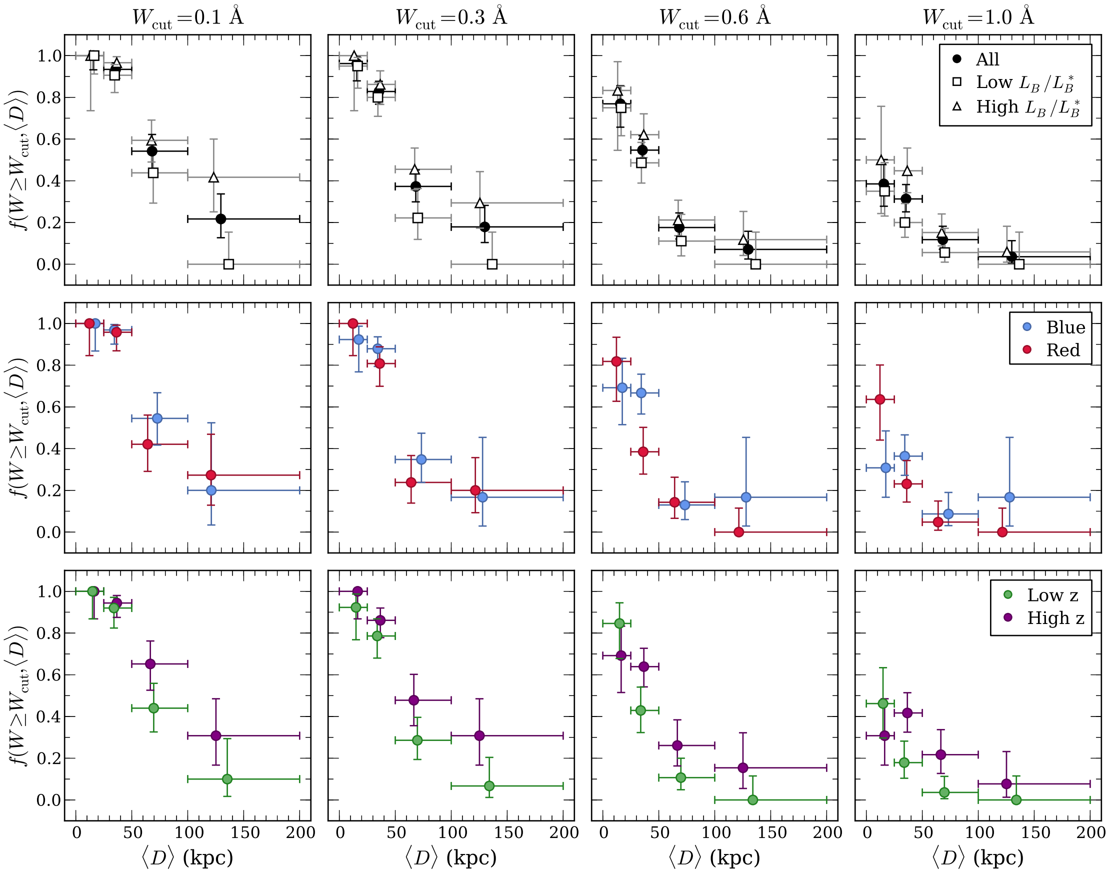

FIG. 3.— The covering fraction profile, $f_{\langle D \rangle}$, for the impact parameter bins $0 \leq D < 25$ kpc, $25 \leq D < 50$ kpc, $50 \leq D < 100$ kpc, and $100 \leq D < 200$ kpc for different $W_r(2796)$ bifurcations at $W_{\rm cut}$. The horizontal bars indicate the impact parameter bin width and the vertical bars are the 1 σ binomial uncertainties. Data points are plotted at the mean impact parameter of the galaxies in the bin. — (upper) The full sample of galaxies (solid points), the high luminosity galaxies (open triangles), and the low luminosity galaxies (open squares). — (middle, lower) Subsamples and colors are the same as given in Figure 2.

dence on galaxy B-band luminosity for $W_{\rm cut}$ = 0.1, 0.3, and 0.5 Å, which is consistent with our result; for $W_{\rm cut}$ = 1.0 Å, we found systematically larger $f_{D\rm max}$ for high luminosity galaxies as compared to low luminosity galaxies, especially for $D_{\rm max} \leq 50$ kpc.

Comparing the fraction of absorbers to non-absorbers as a function of azimuthal angle between the quasar sight line and galaxy major axis, Kacprzak, Churchill, & Nielsen (2012) find $f_{D\rm max} \simeq 70\%$ for $D_{\rm max} \simeq 100$ kpc and $W_{\rm cut}$ = 0.1 Å. Their result is consistent with our finding.

3.4.2. *Covering Fraction Profiles*

To examine the covering fraction profile with projected distance from the galaxy, we computed $f_{\langle D \rangle} \equiv f(W \geq W_{\rm cut}, \langle D \rangle)$, which we define as the fraction of absorbers with $W_r(2796) \geq W_{\rm cut}$ in fixed impact parameter bins. We select the bins $0 \leq D < 25$ kpc, $25 \leq D < 50$ kpc, $50 \leq D < 100$ kpc, and $100 \leq D < 200$ kpc, for which $\langle D \rangle$ is the average impact parameter of the galaxies in the bin.

In Figure 3, we plot $f_{\langle D \rangle}$ against $\langle D \rangle$. The horizontal bars are the impact parameter ranges and the data points are the average impact parameters, $\langle D \rangle$, for each bin. The vertical error bars are the 1 σ uncertainties in $f_{\langle D \rangle}$ based upon binomial statistics. The subsamples presented in each panel are identical to the corresponding panels of Figure 2.

As can be seen in the upper panels of Figure 3, the $f_{\langle D \rangle}$ profile decreases as impact parameter is increased and this behavior is exhibited regardless of $W_{\rm cut}$. Also note that as $W_{\rm cut}$ is increased, $f_{\langle D \rangle}$ is smaller for a given impact parameter bin. This indicates that in a fixed annulus around galaxies,

TABLE 2
LUMINOSITY DEPENDENCE OF COVERING FRACTION PROFILES, $f_{\langle D \rangle}$

$W_{\rm cut}$, Å	(0–25), kpc	[25–50), kpc	[50–100), kpc	[100–200), kpc
		All Galaxies		
0.1	$1.00^{+0.00}_{-0.07}$	$0.93^{+0.03}_{-0.05}$	$0.54^{+0.08}_{-0.08}$	$0.22^{+0.12}_{-0.09}$
0.3	$0.96^{+0.03}_{-0.08}$	$0.83^{+0.05}_{-0.06}$	$0.37^{+0.08}_{-0.07}$	$0.18^{+0.10}_{-0.08}$
0.6	$0.77^{+0.09}_{-0.11}$	$0.55^{+0.07}_{-0.07}$	$0.18^{+0.07}_{-0.06}$	$0.07^{+0.09}_{-0.05}$
1.0	$0.39^{+0.12}_{-0.11}$	$0.31^{+0.07}_{-0.06}$	$0.12^{+0.06}_{-0.05}$	$0.04^{+0.08}_{-0.03}$
		Low L_B/L_B^* Galaxies		
0.1	$1.00^{+0.00}_{-0.09}$	$0.91^{+0.05}_{-0.08}$	$0.44^{+0.15}_{-0.15}$	$0.00^{+0.15}_{-0.00}$
0.3	$0.95^{+0.04}_{-0.11}$	$0.80^{+0.07}_{-0.09}$	$0.22^{+0.14}_{-0.10}$	$0.00^{+0.15}_{-0.00}$
0.6	$0.75^{+0.10}_{-0.13}$	$0.49^{+0.10}_{-0.10}$	$0.11^{+0.13}_{-0.07}$	$0.00^{+0.15}_{-0.00}$
1.0	$0.35^{+0.14}_{-0.12}$	$0.20^{+0.09}_{-0.07}$	$0.06^{+0.12}_{-0.05}$	$0.00^{+0.15}_{-0.00}$
		High L_B/L_B^* Galaxies		
0.1	$1.00^{+0.00}_{-0.26}$	$0.97^{+0.03}_{-0.08}$	$0.59^{+0.10}_{-0.10}$	$0.42^{+0.18}_{-0.17}$
0.3	$1.00^{+0.00}_{-0.26}$	$0.86^{+0.07}_{-0.10}$	$0.46^{+0.10}_{-0.10}$	$0.29^{+0.15}_{-0.12}$
0.6	$0.83^{+0.14}_{-0.29}$	$0.62^{+0.10}_{-0.11}$	$0.21^{+0.10}_{-0.08}$	$0.12^{+0.14}_{-0.08}$
1.0	$0.50^{+0.26}_{-0.26}$	$0.45^{+0.11}_{-0.11}$	$0.15^{+0.09}_{-0.06}$	$0.06^{+0.12}_{-0.05}$

the sky-projected distribution of the Mg II CGM becomes progressively patchier as higher column density material and/or more complex kinematics are selected. For $W_{\rm cut}$ = 0.1 Å, the $f_{\langle D \rangle}$ profile decreases from unity within a radius of 25 kpc to 20% in the annulus 100–200 kpc, whereas for $W_{\rm cut}$ = 1.0 Å, the covering fraction decreases from 40% to less than 10%.

Also shown in the upper panels of Figure 3 is $f_{\langle D \rangle}$ split by $L_B/L_B^* = 0.526$. For low luminosity galaxies, the covering fraction vanishes outside of $D = 100$ kpc for all $W_{\rm cut}$. On the other hand, in the annulus 100–200 kpc, the covering fractions for high luminosity galaxies are approximately 40%, 30%, 10%, and 6% for $W_{\rm cut}$ = 0.1, 0.3, 0.6, and 1.0 Å, respectively. Covering fraction profiles for all, low, and, high luminosity galaxies are listed in Table 2.

The data are suggestive of a luminosity dependence for the maximum extent of Mg II absorbing gas, such that the CGM of low L_B/L_B^* galaxies extends no further than 100 kpc, whereas high luminosity galaxies have a detectable Mg II CGM beyond 100 kpc. The difference between high and low luminosity galaxies is most prominent outside of 50 kpc for $W_{\rm cut}$ = 0.1, and 0.3 Å but is most prominent inside 50 kpc for $W_{\rm cut}$ = 0.6, and 1.0 Å. As such, high luminosity galaxies exhibit a more extended Mg II CGM, whereas for low luminosity galaxies, the Mg II CGM is more concentrated in the central regions but with relatively lower covering fraction as $W_{\rm cut}$ is increased.

In the middle panels of Figure 3, the covering fraction profiles of red and blue galaxies exhibit no significant differences. However, note that for red galaxies, none have absorption with $W_r(2796) \geq 0.6$ Å in the range 100–200 kpc. Blue galaxies consistently have covering fractions of approximately 20% for all $W_{\rm cut}$ in the range 100–200 kpc. However, within 25 kpc the covering fractions for blue galaxies drops more rapidly than for red galaxies with increasing $W_{\rm cut}$. Moreover, for $W_{\rm cut}$ = 0.6 and 1.0 Å there is a weak trend for the covering fraction of red galaxies to drop more rapidly for $D > 25$ kpc relative to the $D =$ 0–25 kpc region. This may suggest that optically thick gas is *relatively* less abundant in the outer regions of redder galaxies as compared to the relative abundance in the outer regions of bluer galaxies.

As shown in the lower panels of Figure 3, high redshift galaxies exhibit a trend of higher $f_{\langle D \rangle}$ in the 25–50, 50–100, and 100–200 kpc annuli relative to low redshift galaxies. Within 25 kpc, the covering fraction may be higher in low redshift galaxies for stronger absorption, $W_{\rm cut}$ = 0.6 and 1.0 Å. Though the trends are marginal, they may suggest a greater extension of the gas at higher redshift followed by a settling of material into the inner regions at lower redshift. However, the behavior of $f_{\langle D \rangle}$ with redshift may be partially influenced by the larger fraction of higher luminosity galaxies at $z \geq \langle z \rangle$.

Chen et al. (2010a) examined $f_{\langle D \rangle}$ for their sample ($\langle z \rangle$ = 0.25), and also found that the covering fraction profile, $f_{\langle D \rangle}$, decreases with increasing D and is smaller at a given $\langle D \rangle$ with increasing $W_{\rm cut}$ using $W_{\rm cut}$ = 0.1, 0.3, and 0.5 Å. However, a direct comparison with our results is difficult because Chen et al. (2010a) scale D assuming a B-band galaxy luminosity dependent "gas radius" proportional to $(L_B/L_B^*)^{0.35}$.

3.5. *Luminosity Scaling and Covering Fraction*

Our results in the previous section strongly suggest that the Mg II absorbing CGM extends further for weaker absorption than for stronger absorption, and that this behavior has a clear dependence with galaxy luminosity. What is further clear, is that for a given $W_{\rm cut}$, the CGM becomes more "patchy" with increasing D, as indicated by the decreasing covering fractions. *As such, it would seem that the notion of a well-defined* Mg II *CGM "gas radius", or "halo absorption radius" is an oversimplification in that the extent of the gas exhibits a "fuzzy" boundary when averaged over many galaxies*. Nonetheless, we parameterize the characteristics of an "outer" boundary and its plausible dependence on the galaxy properties and redshift.

TABLE 3
LUMINOSITY SCALED HALO ABSORPTION RADII

$W_{\rm cut}$ [Å]	*B*-band R_* [kpc]	β	$f_{R(L)}$	*K*-band R_* [kpc]	β	$f_{R(L)}$
0.1	91^{+57}_{-11}	$0.36^{+0.04}_{-0.05}$	$0.89^{+0.03}_{-0.04}$	73^{+45}_{-10}	$0.22^{+0.01}_{-0.03}$	$0.92^{+0.03}_{-0.04}$
0.3	79^{+50}_{-10}	$0.38^{+0.01}_{-0.06}$	$0.84^{+0.04}_{-0.04}$	78^{+38}_{-5}	$0.28^{+0.02}_{-0.09}$	$0.83^{+0.04}_{-0.05}$
0.6	74^{+39}_{-6}	$0.38^{+0.01}_{-0.09}$	$0.61^{+0.05}_{-0.05}$	55^{+38}_{-11}	$0.11^{+0.01}_{-0.01}$	$0.59^{+0.06}_{-0.06}$
1.0	74^{+36}_{-5}	$0.38^{+0.01}_{-0.09}$	$0.34^{+0.05}_{-0.05}$	59^{+34}_{-5}	$0.18^{+0.01}_{-0.03}$	$0.33^{+0.06}_{-0.05}$

Since the work of Bergeron & Boissè (1991), the extent of absorbing gas is commonly assumed to follow a Holmberg-like relation, $R(L) = R_*(L/L^*)^\beta$. We examined whether the halo absorption radius also depends on $W_r(2796)$, and/or galaxy color and redshift.

To examine the dependence on $W_r(2796)$, we adopt $W_{\rm cut}$ = 0.1, 0.3, 0.6, and 1.0 Å. To estimate R_* and β, we varied the two parameters over the ranges $0 \leq R_* \leq 300$ kpc and $0 \leq \beta \leq 1$ and computed the function $q(R_*, \beta, L, W_{\rm cut}) = wr_{(\geq)} + r_{(<)}$, where $r_{(\geq)}$ is the fraction of systems with $W_r(2796) \geq W_{\rm cut}$ below $R(L)$, $r_{(<)}$ is the fraction with $W_r(2796) < W_{\rm cut}$ above $R(L)$, and w is a weighting factor[6]. The parameter values are adopted when $q(R_*, \beta, L, W_{\rm cut})$ is a maximum, for which the covering fraction inside $R(L)$ is $f_{R(L)} = 1/(1+x)$, where $x = (n_{(\geq)}/n_{(<)})(1 - r_{(<)})/r_{(\geq)}$, and where $n_{(\geq)}$ and $n_{(<)}$ are the number of systems with $W_r(2796) \geq W_{\rm cut}$ and $W_r(2796) < W_{\rm cut}$, respectively.

The downward and upward 1 σ uncertainties in R_* were estimated by using the best estimate of β and performing one-sided integration under the $q(R_*, \beta, L, W_{\rm cut})$ curve until 84.13% of the total area was obtained. Similarly, the downward and upward 1 σ uncertainties in β were estimated by using the best estimate of R_*. The 1 σ uncertainties in $f_{R(L)}$ are computed using binomial statistics by computing the fraction of galaxies with $W_r(2796) \geq W_{\rm cut}$ to all galaxies within $R(L)$.

Our results are presented in Table 3 for both B- and K-band luminosities. In the upper panels of Figure 4, we present D against L_B/L_B^*. The luminosity scaling remains roughly constant at $\beta \sim 0.4$ for increasing $W_{\rm cut}$. The absorbing gas halo radius, R_*, for an L_B^* galaxy is on the order of $\sim$ 75 kpc for all but $W_{\rm cut}$ = 0.1 Å, which is on the order of $\sim$ 90 kpc. The covering fraction decreases from $f_{R(L)} = 0.89$ for $W_{\rm cut}$ = 0.1 Å to $f_{R(L)} = 0.34$ for $W_{\rm cut}$ = 1.0 Å.

In the lower panels of Figure 4, we present the K-band results. We note that this subsample has 20 fewer galaxies than the B-band subsample. The luminosity scaling flattens from

---

[6] Since we wish to determine the "outer envelope" of the halo absorption radius, we adopt the weight $w = 2$. When $w = 1$, we find β consistent with zero.

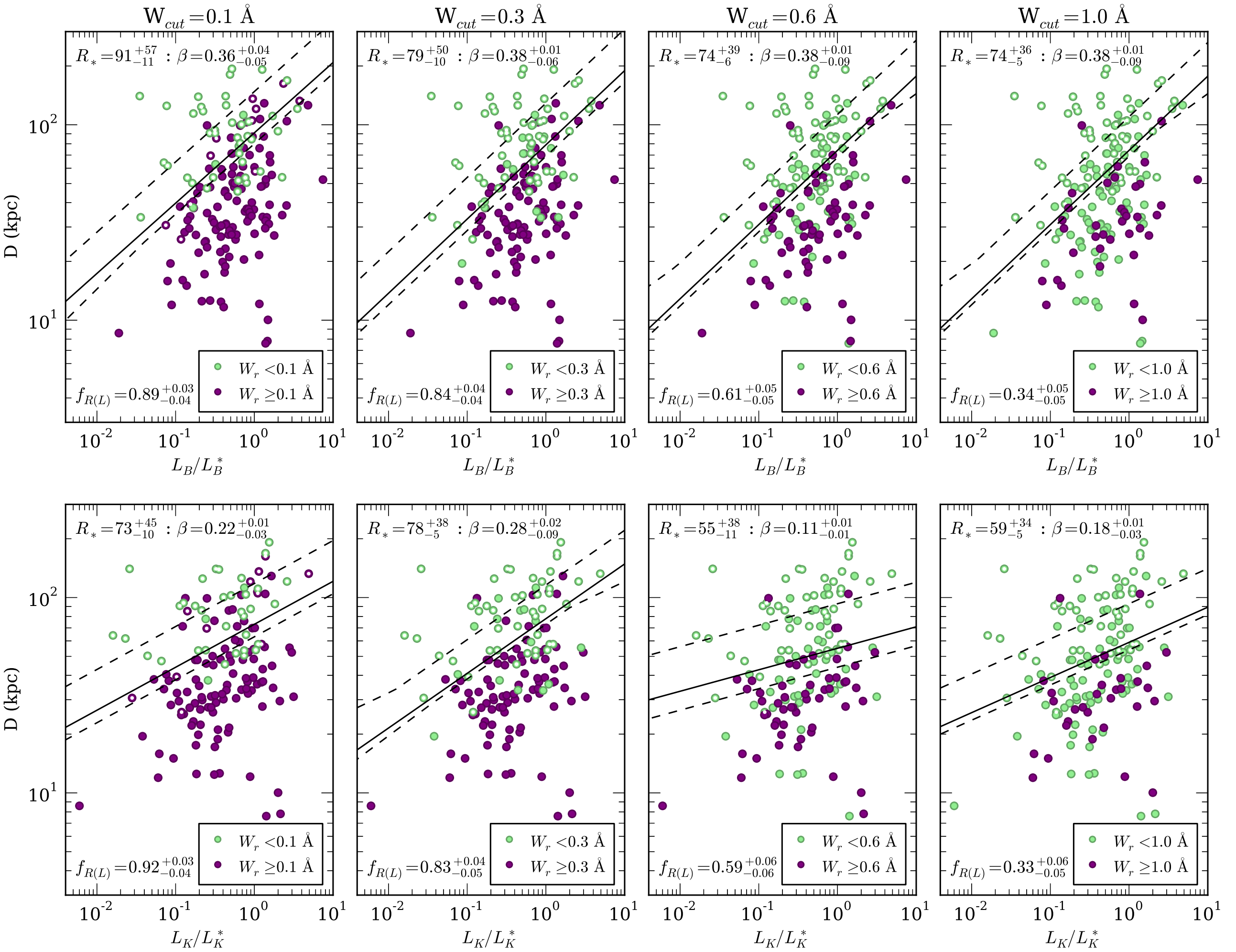

FIG. 4.— Impact parameter, D, versus luminosity for different $W_r(2796)$ bifurcations at $W_{\rm cut}$. Green points are galaxies with $W_r(2796) < W_{\rm cut}$ and purple points are galaxies with $W_r(2796) \geq W_{\rm cut}$. — (upper) B-band luminosity. — (lower) K-band luminosity. Open points represent galaxies which have limits on $W_r(2796)$. The fit parameters R_*, β, and $f_{R(L)}$ give the absorbing gas halo radius for an L^* galaxy, luminosity scaling power index, and absorption covering fraction, respectively, for each $W_r(2796) = W_{\rm cut}$ bifurcation (see Table 3). Dashed lines provide the envelope 1 σ uncertainties in the fit at fixed L/L^*.

$\beta \sim 0.25$ for $W_{\rm cut}$ = 0.1 and 0.3 Å to $\beta \sim 0.15$ for $W_{\rm cut}$ = 0.6 and 1.0 Å, whereas R_* decreases from $\sim$ 75 kpc to $\sim$ 60 kpc. The covering fraction behaves similarly to the B-band (see Table 3).

Steidel (1995) reported $\beta \simeq 0.2$ and R_* = 55 kpc for the B-band and $\beta \simeq 0.15$ and R_* = 58 kpc for the K-band, both for $W_{\rm cut}$ = 0.3 Å (the values of R_* quoted here have been converted to a "737" ΛCDM cosmology at the mean redshift, $\langle z \rangle$ = 0.65, of his sample). He deduced a covering fraction of $f_{R(L)} \simeq 1$ and that β and R_* for the K-band are slightly smaller than for the B-band. Guillemin & Bergeron (1997) obtained similar results, with R_* = 47 kpc (adjusted from q_0 = 0.05 and h_{50} at z = 0.7) and β = 0.28 for the B-band with $W_{\rm cut} \simeq 0.3$ Å.

Using the observed Mg II absorber redshift path number density as a constraint, Kacprzak et al. (2008) explored the parameter space of the minimum luminosity of Mg II absorption-selected galaxies, the slope, β, the halo absorption radius, R_*, and covering fraction, $f_{R(L)}$. For $W_{\rm cut}$ = 0.3 Å, they constrained R_* to the range 50–110 kpc, β to the range 0.2–0.28, and $f_{R(L)}$ to the range 50–80%. Our values of R_* reside in the range of allowed values from their study.

Chen et al. (2010a) reported R_* = 107 kpc with β = 0.35 for the B-band, where they fitted their data in the context of an isothermal sphere model (see Tinker & Chen 2008) of the Mg II CGM. For these values, they find $f_{R(L)}$ = 0.7 for $W_{\rm cut}$ = 0.3 Å and $f_{R(L)}$ = 0.8 for $W_{\rm cut}$ = 0.1 Å, both of which are $\sim$ 10% smaller than what we find.

Employing the Tinker & Chen (2008) isothermal sphere model, Bordoloi et al. (2011) deduced R_* = 115 kpc. Whereas β for this work is consistent with the value reported by Chen et al. (2010a), the larger values of R_* reported by both Chen et al. (2010a) and Bordoloi et al. (2011) may be an artifact of their application of a model to the data. Furthermore, the methods of Bordoloi et al. (2011) involve "averaging" over annuli of fixed impact parameter, which may introduce an additional systematic.

3.5.1. *Galaxy Color*

To examine the dependence of $R(L)$ on galaxy color, we computed R_*, β, and $f_{R(L)}$ for red and blue galaxies, bifurcated by $B-K$ = 1.39, in both the B- and K-bands. Due to the smaller number of galaxies in the blue and red subsamples (74 each), we adopted a single equivalent width cut, $W_{\rm cut}$ = 0.3 Å

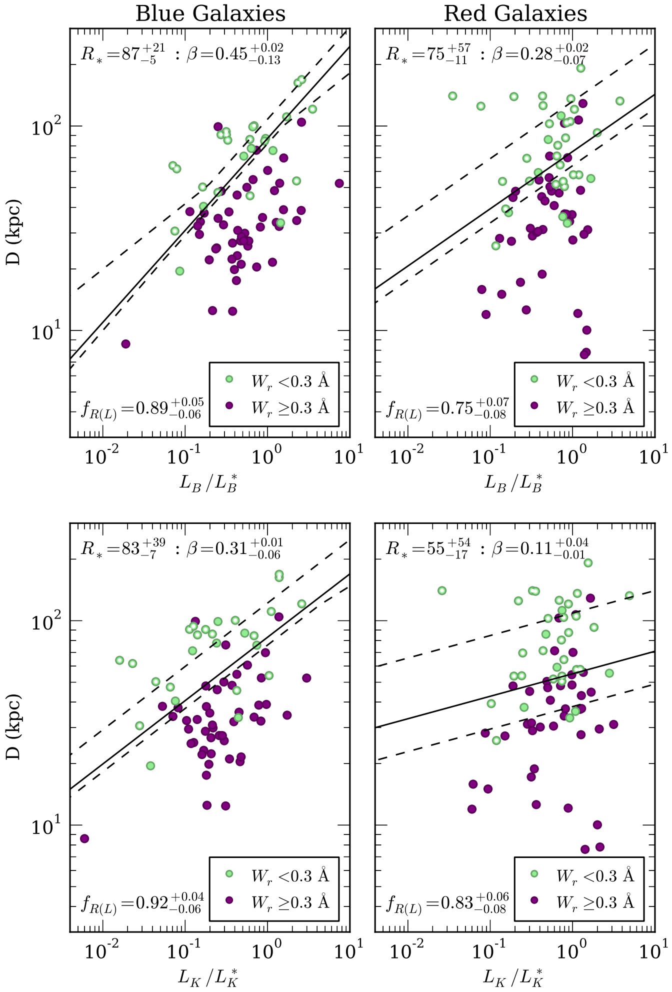

FIG. 5.— Impact parameter, D, versus L_B/L_B^* (top) and L_K/L_K^* (bottom) for blue and red galaxies bifurcated by the median color $B-K = 1.39$. Point types and curves are the same as Figure 4 for $W_{\rm cut} = 0.3$ Å. The luminosity scaling, β, and radius, R_*, of the absorbing gas halo radius exhibits a color dependence for this $W_{\rm cut}$; blue galaxies have a steeper luminosity scaling, larger R_*, and larger covering fraction than red galaxies.

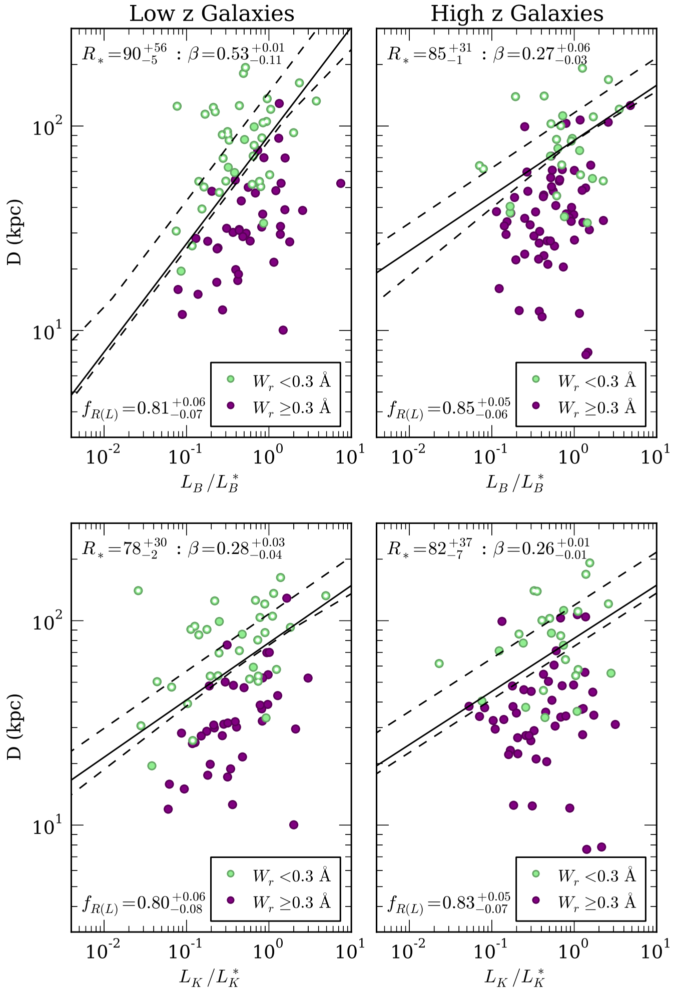

FIG. 6.— Impact parameter, D, versus L_B/L_B^* (top) and L_K/L_K^* (bottom) for low and high redshift galaxies bifurcated by the median redshift $z_{\rm gal} = 0.346$. Point types and curves are the same as Figure 4 for $W_{\rm cut} = 0.3$ Å. The average z for the low redshift subsample is 0.22 and the average for the high redshift subsample is 0.61, which is a ~ 3.2 Gyr difference.

(the median $W_r(2796)$ for galaxies with measured colors). As shown in Figure 5 and tabulated in Table 4, the parameters for $R(L)$ suggest a dependence on galaxy color in both the B- and K-bands.

In the B-band (top panels of Figure 5), we find that blue galaxies have a steeper luminosity scaling, $\beta \sim 0.45$, and larger covering fraction, $f_{R(L)} \sim 0.9$, than red galaxies, $\beta \sim 0.3$ and $f_{R(L)} \sim 0.75$. The halo absorption radius for blue galaxies, $R_* \sim 90$ kpc, is larger than for red galaxies, $R_* \sim 75$ kpc. However, both values of R_* are consistent within uncertainites. These values are smaller than those found by Bordoloi et al. (2011), who report 107 kpc for blue galaxies and 118 kpc for red galaxies. Furthermore, we find the opposite behavior of R_* with color in that our blue galaxies have larger R_* than red galaxies.

The $R(L)$ dependence on galaxy color is similar in the K-band (bottom panels of Figure 5). The halo absorption radius, R_*, is larger for red galaxies (though the values are still consistent within uncertainties), with $R_* \sim 80$ kpc and $R_* \sim 55$ kpc for blue and red galaxies, respectively. The luminosity scaling is steeper in blue galaxies, $\beta \sim 0.3$, than red galaxies, $\beta \sim 0.1$, and the covering fraction is larger in blue galaxies than red galaxies ($f_{R(L)} \sim 0.9$ and $f_{R(L)} \sim 0.8$, respectively).

3.5.2. *Galaxy Redshift*

We also examined the $R(L)$ dependence in both the B- and K-bands on galaxy redshift, bifurcating the sample into low and high redshift galaxies by the median redshift $z = 0.346$, and adopting $W_{\rm cut} = 0.3$ Å. Values for R_*, β, and $f_{R(L)}$ are presented in Figure 6 and tabulated in Table 4.

In the B-band (top panels of Figure 6), we find $R_* \sim 90$ kpc, $\beta \sim 0.5$, and $f_{R(L)} \sim 0.8$ in the low z subsample. The high z subsample has similar values for R_* (~ 85 kpc) and $f_{R(L)}$ (~ 0.85), but a much shallower dependence on L_B/L_B^*, with $\beta \sim 0.3$. This difference in β is driven by the presence of $L_B \simeq 0.1$–$0.4L_B^*$ galaxies with $D \simeq 30$–50 kpc at higher redshift, which are less abundant in the low redshift subsample. It is doubtful that the possible evolution in β is a selection effect, since lower luminosity galaxies would presumably be selected against at high redshift, not lower redshift.

TABLE 4
LUMINOSITY SCALING FOR SUBSAMPLES AT $W_{\rm cut}$ = 0.3 Å

Sample	B-band			K-band		
	R_* [kpc]	β	$f_{R(L)}$	R_* [kpc]	β	$f_{R(L)}$
All	79^{+50}_{-10}	$0.38^{+0.01}_{-0.06}$	$0.84^{+0.04}_{-0.04}$	78^{+38}_{-5}	$0.28^{+0.02}_{-0.09}$	$0.83^{+0.04}_{-0.05}$
Blue	87^{+21}_{-5}	$0.45^{+0.02}_{-0.13}$	$0.89^{+0.05}_{-0.06}$	83^{+39}_{-7}	$0.31^{+0.01}_{-0.06}$	$0.92^{+0.04}_{-0.06}$
Red	75^{+57}_{-11}	$0.28^{+0.02}_{-0.07}$	$0.75^{+0.07}_{-0.08}$	55^{+54}_{-17}	$0.11^{+0.04}_{-0.01}$	$0.83^{+0.06}_{-0.08}$
Low z	90^{+56}_{-5}	$0.53^{+0.01}_{-0.11}$	$0.81^{+0.06}_{-0.07}$	78^{+30}_{-2}	$0.28^{+0.03}_{-0.04}$	$0.80^{+0.06}_{-0.08}$
High z	85^{+31}_{-1}	$0.27^{+0.06}_{-0.03}$	$0.85^{+0.05}_{-0.06}$	82^{+37}_{-7}	$0.26^{+0.01}_{-0.01}$	$0.83^{+0.05}_{-0.06}$

On the other hand, the K-band (bottom panels of Figure 6) shows no discernable difference between the low and high z subsamples. The values for R_*, β, and $f_{R(L)}$ for both subsamples are $\sim$ 80 kpc, $\sim$ 0.3, and $\sim$ 0.8, respectively. Comparing to the apparent B-band evolution, this may imply that the luminosity dependence of the extent of the Mg II absorbing CGM is unchanged with redshift for the K-band.

3.6. *Luminosity Functions*

Prior to measurements of the luminosity functions, $\Phi(M)$, of galaxies out to z = 1 (e.g., Lilly et al. 1995; Lin et al. 1999; Fried et al. 2001; Wolf et al. 2003; Faber et al. 2007; Cirasuolo et al. 2010), selecting galaxies by Mg II absorption provided a compelling technique for compiling a presumably complete sample of intermediate redshift galaxies (Steidel, Dickinson, & Persson 1994). Using absorption selection, Steidel, Dickinson, & Persson (1994) presented the B- and K-band luminosity functions of intermediate redshift galaxies associated with $W_r(2796) \geq 0.3$ Å.

In order to compare to and expand upon the work of Steidel, Dickinson, & Persson (1994), we determined the B- and K-band luminosity functions for MAGIICAT. We divided the galaxies into six subsamples, bifurcated by $W_r(2796)$ = 0.3 Å for all redshifts, low z, and high z. The average redshift for the low z subsample is z = 0.22, and for high z is z = 0.61, which translates to a 3.2 Gyr time spread. Following Steidel, Dickinson, & Persson (1994), we applied a $1/R^2(L)$ correction factor to account for the dependence of gas halo radius on galaxy luminosity, using β = 0.38 for the B-band, and β = 0.28 for the K-band, both from Table 3. This rectifies the relative volume probed by absorption line surveys at fixed luminosity under the assumption of completeness.

In Figures 7 and 8, we present the B- and K-band luminosity functions. For each binned data point, we have computed the mean $B-K$ color of the galaxies contributing to the bin. Blue data points indicate a mean blue color ($B-K < 1.39$) and red points indicate that the mean color is red ($B-K \geq 1.39$). For reference, we have overplotted the Schechter luminosity functions (plus a single additive constant to roughly match the data at M_*) for both z = 0.3 (solid curve) and z = 1.1 (dashed curve) from Faber et al. (2007) for the B-band and Cirasuolo et al. (2010) for the K-band. If the galaxy surveys are magnitude-limited, we estimate that the completeness of MAGIICAT begins to decline for $M_B > -18$ and $M_K > -17.5$ for the low z subsample and $M_B > -19$ and $M_K > -20$ for the high z subsample; these data are conservatively plotted as open points.

3.6.1. *Comparing to Steidel et al. (1994);* $W_r(2796) \geq 0.3$ *Å*

The $W_r(2796) \geq 0.3$ Å subsample at high z (Figure 7f) is most appropriately compared to the Steidel, Dickinson, & Persson (1994) sample. General trends noticeable for galaxies in the B-band associated with $W_r(2796) \geq 0.3$ Å absorption are that there is a slightly higher relative abundance of luminous galaxies in the high z subsample compared to low z (Figures 7f–d), whereas in the K-band, the most luminous galaxies ($M_K < -24.5$) associated with $W_r(2796) \geq 0.3$ Å are not selected in both low and high z subsamples (Figures 8d–f). This is consistent with the correlation between M_B and redshift we found (see § 3.1). For all subsamples, it also appears that the faint-end slope in the B-band may be slightly flatter than the luminosity functions of Faber et al. (2007). In fact, the measured $\Phi(M_B)$ for $W_r(2796) \geq 0.3$ Å at high z (Figure 7f) is suggestive of the turn down at $M_B > -20$, which was reported by Steidel, Dickinson, & Persson (1994).

Apart from the lack of $M_K < -24.5$ galaxies for the $W_r(2796) \geq 0.3$ Å subsamples, the K-band luminosity functions appear to more or less match the luminosity functions of Cirasuolo et al. (2010). We see a possible turnover in the faint-end slope for the $W_r(2796) \geq 0.3$ Å, high z subsample (Figure 8f). This result is contrary to Steidel, Dickinson, & Persson (1994).

For the B-band luminosities, we note that the observed trends (i.e., flattening of the faint-end slope and relative overabundance at high luminosity) are reminiscent of the Malmquist bias that plagues magnitude-limited surveys. Given the heterogeneous selection methods used by the various works from which we constructed MAGIICAT, it is difficult to quantify the degree to which this may be an issue.

3.6.2. *Redshift and* $W_r(2796)$ *Differences*

We ran KS tests on the unbinned data to investigate possible statistical differences between the observed luminosity functions for each subsample. For the B-band, both the $W_r(2796) < 0.3$ Å and $W_r(2796) \geq 0.3$ Å subsamples are consistent with being drawn from the same population, with P(KS) = 0.27 for all redshifts (Figures 7a–b), P(KS) = 0.19 for low z (Figures 7c–d), and P(KS) = 0.42 for high z (Figures 7e–f). The same tests in the K-band yielded similar results for the full sample with P(KS) = 0.41 for all redshifts (Figures 8a–b), P(KS) = 0.66 for low z (Figures 8c–d), and P(KS) = 0.74 for high z (Figures 8e–f).

Comparing the low z and high z subsamples (with mean redshifts of 0.22 and 0.61, respectively, which is a $\sim$ 3.2 Gyr difference), we found evidence for redshift evolution only in the B-band, $\Phi(M_B)$, for the galaxies associated with $W_r(2796) < 0.3$ Å absorption (Figures 7c–e); the test yielded P(KS) = 0.0003 (3.6 σ). This result is due to the absence of luminous galaxies with $M_B \leq -22.5$ and the relative paucity of galaxies with $-22.5 < M_B \leq -21$ at low z, and a lack of lower luminosity galaxies with $M_B > -18$ at high z. The significance level of the KS test may be accentuated by possible magnitude limiting effects in the high z subsample (but the bright end would not be related to this plausible selection effect).

The same trend is also apparent for the $W_r(2796) \geq 0.3$ Å subsample in the B-band (Figures 7d–f). However, the result is not formally significant; the KS test yielded a 91% CL (1.7 σ). For $\Phi(M_K)$, there is no suggestion of redshift evolution for both the $W_r(2796) < 0.3$ and $W_r(2796) \geq 0.3$ subsamples.

3.6.3. *Color Sequence Along* $\Phi(M_B)$ *and* $\Phi(M_K)$

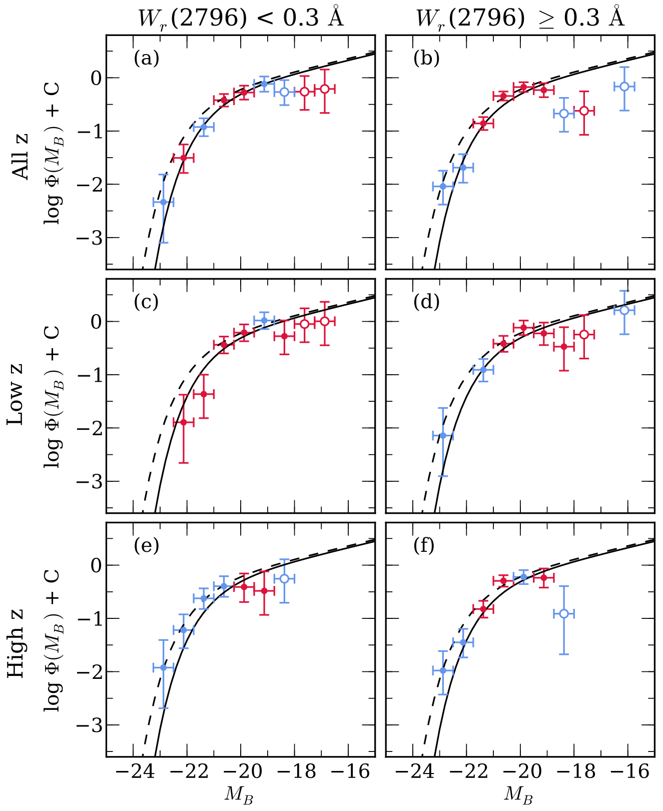

FIG. 7.— *B*-band luminosity functions for $W_r(2796) < 0.3$ (*a*, *c*, and *e*) and $W_r(2796) \geq 0.3$ (*b*, *d*, and *f*). Galaxies at all redshifts are included in panels *a* and *b*, while galaxies with $z < \langle z \rangle$ are in panels *c* and *d* (mean $z = 0.22$), and galaxies with $z \geq z\rangle$ are in panels *e* and *f* (mean $z = 0.61$), where $\langle z \rangle = 0.346$. The solid and dashed curves are $z = 0.3, 1.1$ Schechter functions, respectively, from Faber et al. (2007). Data points are colored according to the mean color of the galaxies in the bin. Blue points correspond to a mean color $B-K < 1.39$ and red data points correspond to $B-K \geq 1.39$. Open points are where the completeness of the sample declines.

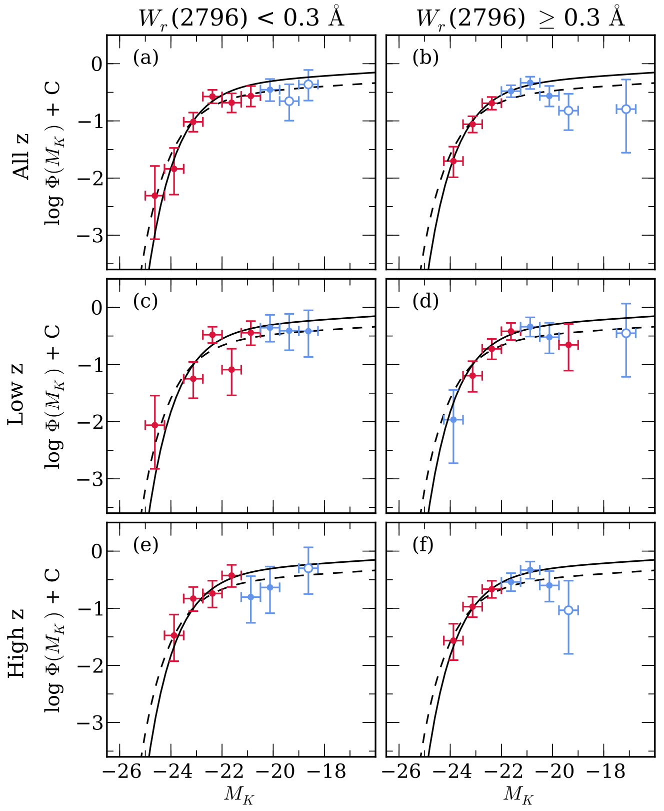

FIG. 8.— *K*-band luminosity functions for $W_r(2796) < 0.3$ (*a*, *c*, and *e*) and $W_r(2796) \geq 0.3$ (*b*, *d*, and *f*). Galaxies at all redshifts are included in panels *a* and *b*, while galaxies with $z < \langle z \rangle$ are in panels *c* and *d* (mean $z = 0.22$), and galaxies with $z \geq \langle z \rangle$ are in panels *e* and *f* (mean $z = 0.61$), where $\langle z \rangle = 0.346$. The solid and dashed curves are $z = 0.3, 1.1$ Schechter functions, respectively, from Cirasuolo et al. (2010). Point types are the same as described in Figure 7.

For the *B*-band, it is somewhat striking that, for high *z* galaxies associated with $W_r(2796) < 0.3$ Å (Figure 7*e*), the mean color trends toward bluer galaxies for a wide range of luminosities. Yet, at low *z*, the mean color of the galaxies associated with $W_r(2796) < 0.3$ Å absorption (Figure 7*c*) trends toward redder galaxies. For $W_r(2796) \geq 0.3$ Å, galaxies fainter than M_B^* trend red at lower *z* (Figure 7*d*). However, the color sequence along $\Phi(M_B)$ for the low redshift and high redshift subsamples (Figures 7*d* and 7*f*) show no clear redshift trend.

Steidel, Dickinson, & Persson (1994) reported a correlation between M_K and $B-K$ such that lower luminosity galaxies in the *K*-band tend to be more blue. Performing a Kendall's τ rank correlation test on M_K versus $B-K$ for the full sample of galaxies presented here yielded a 6.3 σ correlation. For the *K*-band, the trend for lower luminosity galaxies to be bluer is clearly seen in the color sequence of $\Phi(M_K)$ for all redshift and $W_r(2796)$ subsamples (consistent with the correlation tests on M_K versus $B-K$). There is no correlation between $B-K$ and M_B.

To further explore the data, we bifurcated the sample at (1) $W_{\rm cut} = 0.3$ Å, (2) $z = 0.346$, and (3) $L_B/L_B^* = 0.526$. The Kendall tests on M_K versus $B-K$ for these subsamples resulted in significant correlations in all cases, with the most significant results for low L_B/L_B^* (5.9 σ), high *z* (5.3 σ), and $W_r(2796) \geq 0.3$ (4.6 σ). These subsamples all correspond to the faint end of $\Phi(M_K)$ shown in Figure 8*f*.

4. DISCUSSION

With the larger sample afforded by MAGIICAT, we have obtained additional leverage to probe the dependence of the properties of the Mg II absorbing CGM with galaxy color, luminosity, impact parameter, and $W_r(2796)$ threshold. For our analysis, we have purposely avoided couching the data within the framework of model expectations or scaling various measured quantities with "second parameters", such as scaling the impact parameter by galaxy luminosity, in order to provide a direct view of the CGM-galaxy connection and to interpret the data from a purely observational perspective.

With regard to the relationship between galaxy color and $W_r(2796)$, our results challenge those of previous studies. For the overall sample, we find no correlation between $W_r(2796)$ and $B-K$. However, we find that for the subsample with $W_r(2796) \geq 1$ Å, redder galaxies have larger $W_r(2796)$ with a significance level of 3.1 σ. These findings are contrary to the results of Zibetti et al. (2007) and Bordoloi et al. (2011), who both report larger $W_r(2796)$ associated with bluer galaxies. It is difficult to rectify the inconsistencies of our findings with those works unless the solution originates in the different experimental methods.

Zibetti et al. (2007) developed an image stacking method in which the individual galaxies are not identified, but light from galaxies in various SDSS photometric bands are measured *rel-*

ative to control fields for which the quasars show no Mg II absorption. They employ observer-frame colors, whereas we examine rest-frame colors including the K-band. The color cuts of the galaxies studied by Bordoloi et al. (2011) are based upon a color-mass relation using $u-B$ colors. Furthermore, the equivalent widths measured by Bordoloi et al. (2011) are based on stacked spectra over fixed impact parameter annuli in which the Mg II doublet is not resolved, whereas those measured in this work are based upon pencil-beam probes of the CGM for which all doublets are cleanly resolved. If the CGM is intrinsically patchy (see Churchill et al. 2012a) with covering fraction dependencies on $W_r(2796)$ threshold and galaxy luminosity (as we have demonstrated in this paper), then the two methods (statistical versus case-by-case) may be providing complimentary but different clues to the nature of the CGM.

Our analysis of the covering fraction profile of the Mg II absorbing CGM as a function of impact parameter, galaxy luminosity, and absorption strength threshold provides improved insights on the extent and distribution of the low ionization, metal-enriched CGM (see Figure 3 and Table 2). The decrease in the covering fraction with increasing absorption threshold indicates that the cross-section of the highest column density and/or most kinematically dispersed gas (plausibly winds material) is smaller than the cumulative cross-section including lower column density, kinematically quiescent gas (plausibly accretion material).

Additional insight is provided by the relative behavior of the covering fraction profile of low and high luminosity galaxies (bifurcated at $L_B/L_B^* = 0.526$). First, the Mg II absorbing CGM appears to extend no further than 100 kpc for low luminosity galaxies. Second, the CGM at $D \geq 100$ kpc surrounding high luminosity galaxies is dominated by lower column density, kinematically quiescent gas traced by $W_r(2796) < 0.6$ Å absorption; the cross-section of this material increases as the equivalent width threshold is decreased to 0.1 Å. This trend is also seen in the range $50 < D \leq 100$ kpc. In contrast, in the range $D < 50$ kpc, the observed frequencies of lower and higher column density CGM gas is not strongly dependent on galaxy luminosity for $W_r(2796) < 0.6$ Å, but for $W_r(2796) \geq 0.6$ Å, high luminosity galaxies have a higher observed frequency of Mg II absorbing CGM. This difference is most highly apparent for $W_r(2796) \geq 1.0$ Å. Within $D = 25$ kpc, the covering fraction is effectively unity for the thresholds $W_r(2796) \geq 0.1$ and 0.3 Å, but declines for $W_r(2796) \geq 0.6$ and 1.0 Å as the threshold is increased.

These results indicate a strong luminosity dependence in cross-sections and extent of the Mg II absorbing CGM such that high luminosity galaxies have both a much more extended diffuse CGM than low luminosity galaxies and higher filling factors of the highest column density material within 50 kpc as compared to low luminosity galaxies. Since the luminosity segregation we are employing is for the B-band, we could be seeing a connection between the CGM and young stars, such that the increased presence of young stars is related to a greater cross-section of higher column density gas in the inner regions of the galaxies and a more extended distribution of the lower column density gas in the outer regions of the galaxies (beyond 100 kpc). This would imply a stellar driven mechanism for distributing the gas in the CGM.

Following previous studies, we have assumed the relation $R(L) = R_*(L/L^*)^\beta$ to describe the "halo absorption radius" dependence on luminosity. For the B-band luminosity, we find that the sensitivity of $R(L)$ to luminosity (the parameter β, see Table 3 and Figure 4) does not change as the equivalent width threshold is raised. For $W_r(2796) \geq 0.1$ we find $\beta \simeq 0.36$, and for $W_r(2797) \geq 0.3$, 0.6, and 1.0 Å, we find $\beta \simeq 0.38$. However, the extent for an L_B^* galaxy tends to decrease as the equivalent width threshold is raised. We find $R_* \simeq 90$ kpc for $W_r(2796) \geq 0.1$ Å, $R_* \simeq 80$ kpc for $W_r(2796) \geq 0.3$ Å, and $R_* \simeq 75$ kpc for $W_r(2796) \geq 0.6$ and 1.0 Å.

Interestingly, we find a shallower dependence of $R(L)$ on the K-band luminosity. Contrary to the B-band, the value of β tends to decrease as the equivalent width threshold is increased (though not monotonically). Furthermore, we find smaller R_* for the K-band than for the B-band.

The greater extent and higher luminosity sensitivity to the B-band relative to the K-band would further strengthen the idea that the geometric extent and morphology of the Mg II absorbing CGM is governed in large part by young stars. There is an indication that galaxy color directly plays a role in governing the higher B-band luminosity sensitivity of $R(L)$. For $W_r(2797) \geq 0.3$ Å, blue galaxies have a remarkably steeper luminosity dependence than do red galaxies. For blue galaxies, we find $\beta \simeq 0.45$ for the B-band and $\beta \simeq 0.30$ for the K-band, whereas for red galaxies, we find $\beta \simeq 0.28$ for the B-band and $\beta \simeq 0.11$ for the K-band. In the B-band, the covering fraction within $R(L)$ of red galaxies is $\simeq 15\%$ lower than for blue galaxies, whereas it is only $\simeq 10\%$ lower in the K-band.

We strongly caution that the function $R(L)$ should not be viewed as a well-defined outer boundary to the Mg II absorbing CGM. Examination of the data on the D–L/L^* plane shown in Figure 4 clearly reveals that a non-negligible number of galaxies with $W_r(2796)$ greater than the threshold cut also reside above the curve. The 1 σ upper envelope of the $R(L)$ boundary characterizes the presence of these galaxies. These galaxies also drive the large upward uncertainties in best fit R_*. Note that this uncertainty increases from $\simeq 36$ to $\simeq 57$ kpc as the absorption threshold is decreased from $W_r(2796) \geq 1.0$ to 0.1 Å. This suggests that the $R(L)$ boundary is less well defined for the lower column density structures of the CGM. Physically, the behavior of the data in this regime of impact parameter and $W_r(2796)$ could either reflect a greater level of patchiness in the low column density material residing in the outskirts of the CGM of individual galaxies or a broad range of CGM properties from galaxy to galaxy.

The color sequence across the B- and K-band luminosity functions indicates relationships between $W_r(2796)$, redshift, and galaxy luminosity that might otherwise not have been discovered in the data without a multivariate analysis. At high z, $W_r(2796) < 0.3$ Å absorption is associated primarily with galaxies for which the mean color is blue ($B-K < 1.39$) across the full B-band luminosity range. Interestingly, we find the mean colors of the low z galaxies associated with $W_r(2796) < 0.3$ Å absorption have an average color that is primarily red. For $W_r(2796) \geq 0.3$ Å, the data may suggest that the reddening of galaxies with decreasing redshift occurs at sub-L_B^* luminosities.

Comparing to the luminosity functions of Steidel, Dickinson, & Persson (1994), we see possible evidence for a faint-slope turnover in the B-band for the appropriate subsample of galaxies in MAGIICAT (see Figure 7f). Interestingly, we also see possible evidence for a faint-slope turnover in the corresponding K-band luminosity function at the faint end (see Figure 8f). This latter result is contrary to the findings of Steidel, Dickinson, & Persson

(1994). Given the heterogeneous selection of the galaxies for MAGIICAT, it is difficult to assess if these turnovers are influenced by incompleteness at low luminosities at higher redshift.

5. CONCLUSION

Combining our previous studies and the extant works in the literature, we have compiled a "Mg II Absorber-Galaxy Catalog" (MAGIICAT) of intermediate redshift galaxies and their associated circumgalactic medium (CGM) as probed using Mg II $\lambda\lambda 2796, 2803$ absorption. Details of the MAGIICAT data will be presented in Paper I. In this paper, we present results from a first analysis, focusing exclusively on "isolated" galaxies, which are defined to have no neighboring galaxy within a projected distance of 100 kpc and line of sight velocity within 500 km s^{-1}.

The sample presented here comprises 169 galaxies toward 117 quasar sightlines over the redshift range $0.072 \leq z_{\rm gal} \leq 1.120$, with median $\langle z \rangle = 0.346$. The rest-frame magnitudes range from $-16.1 \geq M_B \geq -22.8$ ($0.017 \leq L_B/L_B^* \leq 7.44$) and $-17.0 \geq M_K \geq -24.3$ ($0.006 \leq L_K/L_K^* \leq 4.9$) with AB rest-frame colors $0.04 \leq B-K \leq 4.09$. The median B-band luminosity is $L_B/L_B^* = 0.526$ and the median color is $B-K = 1.39$.

The main results are:

1. The $B-K$ color exhibits a trend to redden with decreasing redshift, but the reddening is not statistically significant (2.3 σ). The mean M_B increases with increasing redshift (4.4 σ), whereas M_K exhibits a weak trend to increase with redshift (2.1 σ). The subsample with $W_r(2796) \geq 0.8$ Å is highly consistent with no color evolution, in conflict with the result of Zibetti et al. (2007); however, the subsample with $W_r(2796) < 0.8$ Å shows a reddening trend with decreasing redshift (2.5 σ), suggesting the reddening trend we see is dominated by galaxies with $W_r(2796)$ below the sensitivity of Zibetti et al. (2007).

2. There is no correlation between $W_r(2796)$ and $B-K$ for the full sample (1.1 σ). However, for galaxies associated with $W_r(2796) \geq 1.0$ Å absorption, $B-K$ correlates with $W_r(2796)$ at 3.1 σ, indicating that redder galaxies have stronger absorption in this equivalent width regime. In our sample, the distributions of $W_r(2796)$ within $D = 50$ kpc of blue ($B-K < 1.39$) and red ($B-K \geq 1.39$) galaxies are consistent with being drawn from the same parent distribution (0.5 σ). The $W_r(2796)$-color correlation in our sample conflicts with the $W_r(2796)$-color anti-correlation reported by Zibetti et al. (2007). Both the $W_r(2796)$-color correlation and the indistinguishable $W_r(2796)$ distributions in our sample are in conflict with the findings of Bordoloi et al. (2011), who report eight times stronger $W_r(2796)$ within $D = 50$ kpc associated with bluer galaxies.

3. Including upper limits on $W_r(2796)$, we find that the significance level of the well-known anti-correlation between $W_r(2796)$ and impact parameter, D, is 8.2 σ for this sample. The best parameterization is a log-linear relation, for which we find $\log W_r(2796) = (-0.019 \pm 0.002)D + (0.28 \pm 0.11)$. The scatter in this relation may be due to the redshifts, colors, or luminosities of the galaxies. Bifurcations in these galaxy properties result in at most a $\sim 3.3\,\sigma$ correlation where higher K-band luminosity galaxies tend to have higher $W_r(2796)$ at a given impact parameter. Dividing the sample into quartiles based on the redshift, color, or luminosity of the galaxies and comparing the lowest and highest quartiles gives at best a $\sim 2.5\,\sigma$ correlation with B-band luminosity.

4. The covering fraction profiles with projected distance from the galaxy, $f_{D\rm max}$ and $f_{\langle D \rangle}$, decrease with both increasing D and increasing minimum $W_r(2796)$ (see Figures 2 and 3). High luminosity galaxies have higher covering fractions. In terms of $f_{\langle D \rangle}$, this difference is greatest at $100 < D \leq 200$ kpc for absorbing CGM gas with $W_r(2796) \geq 0.1$ Å and at $D \leq 50$ kpc for CGM gas with $W_r(2796) \geq 1.0$ Å. There is no clear difference between the covering fraction profile of blue galaxies versus red galaxies. The high redshift galaxies ($z \geq \langle z \rangle$) have a higher covering fraction than the low redshift galaxies ($z < \langle z \rangle$) at $D > 50$ kpc. Since our sample comprises a larger fraction of high luminosity galaxies at high redshift, this latter result may be tracing the luminosity dependence of the covering fraction. A multivariate analysis would be useful for examining such possible cross-correlations in the sample.

5. We determined the best-fit parameters R_* and β for the luminosity scaling of the outer envelope for absorption, or the "halo absorption radius", $R(L) = R_*(L/L^*)^\beta$, for both the B- and K-bands as a function of $W_r(2796)$ threshold. For the B-band, the luminosity scaling remains roughly constant at $\beta \sim 0.4$ with increasing $W_{\rm cut}$. We find $R_* \sim 75$ kpc for all but $W_{\rm cut} = 0.1$ Å, which is on the order of ~ 90 kpc. The covering fraction inside $R(L_B)$ decreases from $f_{R(L)} = 0.89$ for $W_{\rm cut} = 0.1$ Å to $f_{R(L)} = 0.34$ for $W_{\rm cut} = 1.0$ Å. For the K-band, the luminosity scaling flattens from $\beta \sim 0.25$ for $W_{\rm cut} = 0.1$ and 0.3 Å to $\beta \sim 0.15$ for $W_{\rm cut} = 0.6$ and 1.0 Å, whereas R_* decreases from ~ 75 kpc to ~ 60 kpc. The covering fraction behaves similarly to the B-band. Though the "outer envelope" for absorption has a clear dependence on both luminosity and $W_r(2796)$ threshold, we note that the scatter in the data in the $W_r(2796)$-D plane, the behavior of the covering fraction profile $f_{\langle D \rangle}$ with increasing D, and the relatively extended upward uncertainties in R^* all indicate that $R(L)$ is not a well-defined quantity, but should be interpreted as a "fuzzy" boundary and that the "fuzziness" increases with decreasing equivalent width threshold.

6. Dividing the galaxies by the median color ($B-K = 1.39$), adopting $W_{\rm cut} = 0.3$ Å, and examining the fit parameters to $R(L) = R_*(L/L^*)^\beta$, we find that, in the B-band, blue galaxies have a steeper luminosity scaling, $\beta \sim 0.45$, and larger covering fraction, $f_{R(L)} \sim 0.9$, than red galaxies, $\beta \sim 0.3$ and $f_{R(L)} \sim 0.75$. The halo absorption radius for blue galaxies, $R_* \sim 90$ kpc, is larger than for red galaxies, $R_* \sim 75$ kpc. Our results are in conflict with the results of Bordoloi et al. (2011).

7. We also examined the $R(L)$ dependence in both the B- and K-bands on galaxy redshift, bifurcating the sample at the median redshift $z = 0.346$, and adopting $W_{\rm cut} = 0.3$ Å. In the B-band, we find $R_* \sim 90$ kpc, $\beta \sim 0.5$, and $f_{R(L)} \sim 0.8$ in the low z subsample. The high z subsample has similar values for R_* (~ 85 kpc) and $f_{R(L)}$ (~ 0.85), but a much shallower dependence on L_B/L_B^*, with $\beta \sim 0.3$. In the K-band, we find no discernable difference between the low and high z subsamples. The values for R_*, β, and $f_{R(L)}$ for both subsamples are ~ 80 kpc, ~ 0.3, and ~ 0.8, respectively.

8. We present the B- and K-band luminosity functions, $\Phi(M)$, for subsamples split by $W_r(2796) < 0.3$ Å and $W_r(2796) \geq 0.3$ Å and by low z and high z. For all subsamples, the faint-end slope in the B-band may be slightly flatter than the luminosity functions of Faber et al. (2007). $\Phi(M_B)$ for $W_r(2796) \geq 0.3$ Å at high z is suggestive of the turn down at $M_B > -20$, which was reported by Steidel, Dickinson, & Persson (1994). Comparing the low z

and high z subsamples, we found evidence for redshift evolution (3.6 σ) in the B-band for the galaxies associated with $W_r(2796) < 0.3$ Å absorption. In addition, for high z galaxies associated with $W_r(2796) < 0.3$ Å, the mean color trends toward bluer galaxies, but at low z, the mean color trends toward redder galaxies. For $W_r(2796) \geq 0.3$ Å, the color sequence along $\Phi(M_B)$ for the low redshift and high redshift subsamples shows no clear redshift trend. We also find a 6.3 σ correlation between M_K and $B-K$ such that lower luminosity galaxies in the K-band tend to be bluer (consistent with Steidel, Dickinson, & Persson 1994).

This work constitutes our first examination of the relationship of the Mg II absorbing CGM with galaxy properties using MAGIICAT. In particular, we have examined the data by comparing direct observables and have avoided analyzing the quantities based upon converting or scaling the data to a preferred model of the CGM. Our aim has been to provide an unfiltered view of the Mg II absorbing CGM. Nonetheless, the simple bivariate testing we have conducted here does not provide full leverage for probing of the available data. In future work, we will apply multivariate analysis methods in which we also incorporate mass estimates of the galaxies (see Churchill et al. 2012b), Mg II kinematics, and both low and high ionization absorption strengths of the CGM for these galaxies. We will also conduct comparative studies of the isolated galaxies and group galaxies in the catalog.

We thank Chuck Steidel for communicating detailed aspects related to the work by Steidel, Dickinson, & Persson (1994), including access to unpublished materials. We also extend our gratitude to all the researchers whose hard work over the last two decades resulted in the growing database of published galaxies in quasar fields. Without their efforts, this work would not have been possible. We thank Nick Gnedin for reading and providing insightful comments on an earlier draft. This research was primarily supported through grant HST-AR-12646 provided by NASA via the Space Telescope Science Institute, which is operated by the Association of Universities for Research in Astronomy (AURA) under NASA contract NAS 5-26555. This work was also supported by the Research Enhancement Program provided by NASA's New Mexico Space Grant Consortium (NMSGC). NMN was also partially supported through a NMSGC Graduate Fellowship and a Graduate Research Enhancement Grant (GREG) sponsored by the Office of the Vice President for Research at New Mexico State University. This research has made extensive use of the SAO/NASA Astrophysics Database System (ADS), operated by the Smithsonian Astrophysical Observatory under contract with NASA, the NASA/IPAC Extragalactic Database (NED), operated by the Jet Propulsion Laboratory and California Institute of Technology, under contract with NASA, and the SIMBAD database, operated at Centre de Données, Strasbourg, France.

REFERENCES

Adelberger, K. L., Shapley, A. E., Steidel, C. C., et al. 2005, ApJ, 629, 636

Barton, E. J., & Cooke, J. 2009, AJ, 138, 1817

Bechtold, J., & Ellingson, E. 1992, ApJ, 396, 20

Benjamin, R. A., & Danly, L. 1997, ApJ, 481, 764

Bergeron, J., & Boissè, P. 1991, A&A, 243, 334

Bergeron, J., & Stasińska, G. 1986, A&A, 169, 1

Birnboim, Y., & Dekel, A. 2003, MNRAS, 345, 349

Birnboim, Y., Dekel, A., & Neistein, E. 2007, MNRAS, 380, 339

Bolzonella, M., Miralles, J.-M., & Pelló, R. 2000, A&A, 363, 476

Bordoloi, R., Lilly, S. J., Knobel, C., et al. 2011, ApJ, 743, 10

Bouché, N., Hohensee, W., Vargas, R., et al. 2011, MNRAS, in press (arXiv:1110.5877)

Bouché, N., Murphy, M. T., Péroux, C., Csabai, I., & Wild, V. 2006, MNRAS, 371, 495

Brown, B. W., Hollander, M., & Korwar, R. M. 1974, in Reliability and Biometry, 327

Bruzual A. G., & Charlot, S. 1993, ApJ, 405, 538

Charlton, J. C., & Churchill, C. W. 1996, ApJ, 465, 631

Chelouche, D., & Bowen, D. V. 2010, ApJ, 722, 1821

Ceverino, D., & Klypin, A. 2009, ApJ, 695, 292

Charlton, J. C., & Churchill, C. W. 1998, ApJ, 499, 181

Chen, H.-W., Helsby, J. E., Gauthier, J.-R., Shectman, S. A., Thompson, I. B., & Tinker, J. L. 2010a, ApJ, 714, 1521

Chen, H.-W., Lanzetta, K. M., & Webb, J. K. 2001a, ApJ, 556, 158

Chen, H.-W., Lanzetta, K. M., Webb, J. K., & Barcons, X. 2001b, ApJ, 559, 654

Chen, H.-W., Wild, V., Tinker, J. L., et al. 2010b, ApJ, 724, L176

Chen, H.-W., & Tinker, J. L. 2008, ApJ, 687, 745

Churchill, C. W., Kacprzak, G. G., Nielsen, N. M., Steidel, C. C., Murphy, M. T. 2012a, ApJ, submitted

Churchill, C. W., Kacprzak, G. G., & Steidel, C. C. 2005, IAU Colloq. 199: Probing Galaxies through Quasar Absorption Lines, 24

Churchill, C. W., Kacprzak, G. G., Steidel, C. C., & Evans, J. L. 2007, ApJ, 661, 714

Churchill, C. W., Mellon, R. R., Charlton, J. C., Jannuzi, B. T., Kirhakos, S., Steidel, C. C., & Schneider, D. P. 2000a, ApJS, 130, 91

Churchill, C. W., Mellon, R. R., Charlton, J. C., et al. 2000b, ApJ, 543, 577

Churchill, C. W., Nielsen, N. M., Kacprzak, G. G., & Trujillo-Gomez, S. 2012b, ApJL, submitted (Paper III)

Churchill, C. W., Rigby, J. R., Charlton, J. C., & Vogt, S. S. 1999, ApJS, 120, 51

Churchill, C. W., Steidel, C. C., & Vogt, S. S. 1996, ApJ, 471, 164

Churchill, C. W., & Vogt, S. S. 2001, AJ, 122, 679

Churchill, C. W., Vogt, S. S., & Charlton, J. C. 2003, AJ, 125, 98

Cirasuolo, M., McLure, R. J., Dunlop, J. S., Almaini, O., Foucaud, S., & Simpson, C. 2010, MNRAS, 401, 1166

Coleman, G. D., Wu, C.-C., & Weedman, D. W. 1980, ApJS, 43, 393

Dekel, A., & Birnboim, Y. 2006, MNRAS, 368, 2

Dekel, A., & Silk, J. 1986, ApJ, 303, 39

Evans, J. L. 2011, Ph.D. Thesis, New Mexico State University

Faber, S. M., et al. 2007, ApJ, 665, 265

Fried, J. W., von Kuhlmann, B., Meisenheimer, K., et al. 2001, A&A, 367, 788

Gauthier, J.-R., Chen, H.-W., & Tinker, J. L. 2009, ApJ, 702, 50

Gehrels, N. 1986, ApJ, 303, 336

Guillemin, P., & Bergeron, J. 1997, A&A, 328, 499

Kacprzak, G. G., & Churchill, C. W. 2011, ApJ, 743, L34

Kacprzak, G. G., Churchill, C. W., Barton, E. J., & Cooke, J. 2011a, ApJ, 733, 105

Kacprzak, G. G., Churchill, C. W., Ceverino, D., et al. 2010, ApJ, 711, 533

Kacprzak, G. G., Churchill, C. W., Evans, J. L., Murphy, M. T., & Steidel, C. C. 2011b, MNRAS, 416, 3118

Kacprzak, G. G., Churchill, C. W., Nielsen, N. M. 2012, ApJ, 760, L7

Kacprzak, G. G., Churchill, C. W., Steidel, C. C., & Murphy, M. T. 2008, AJ, 135, 922

Kacprzak, G. G., Churchill, C. W., Steidel, C. C., Murphy, M. T., & Evans, J. L. 2007, ApJ, 662, 909

Kacprzak, G. G., Churchill, C. W., Steidel, C. C., Spitler, L. R., & Holtzman, J. A. 2012, MNRAS, accepted (arXiv:1208.4098)

Kacprzak, G. G., Murphy, M. T., & Churchill, C. W. 2010, MNRAS, 406, 445

Kereš, D., Katz, N., Fardal, M., Davé, R., & Weinberg, D. H. 2009, MNRAS, 395, 160

Kereš, D., Katz, N., Weinberg, D. H., & Davé, R. 2005, MNRAS, 363, 2

Kim, A., Goobar, A., & Perlmutter, S. 1996, PASP, 108, 190

Lanzetta, K. M., & Bowen, D. 1990, ApJ, 357, 321

Lanzetta, K. M., & Bowen, D. V. 1992, ApJ, 391, 48

Lanzetta, K. M., Bowen, D. V., Tytler, D., & Webb, J. K. 1995, ApJ, 442, 538

Le Brun, V., Bergeron, J., Boisse, P., & Christian, C. 1993, A&A, 279, 33

Lilly, S. J., Tresse, L., Hammer, F., Crampton, D., & Le Fevre, O. 1995, ApJ, 455, 108

Lin, H., Yee, H. K. C., Carlberg, R. G., et al. 1999, ApJ, 518, 533

Maller, A. H., & Bullock, J. S. 2004, MNRAS, 355, 694

Martin, C. L., & Bouché, N. 2009, ApJ, 703, 1394

McGuagh, S. S., Schombert, J. M., de Blok, W. J. G., & Zagursky, M. J. 2010, ApJ, 708, L14

Ménard, B., Wild, V., Nestor, D., et al. 2011, MNRAS, 417, 801

Mo, H. J., & Miralda-Escude, J. 1996, ApJ, 469, 589

Narayanan, A., Misawa, T., Charlton, J. C., & Kim, T.-S. 2007, ApJ, 660, 1093

Navarro, J. F., Frenk, C. S., & White, S. D. M. 1996, ApJ, 462, 563

Nestor, D. B., Turnshek, D. A., & Rao, S. M. 2005, ApJ, 628, 637

Nielsen, N. M., Churchill, C. W., Kacprzak, G. G. 2013, ApJS, in prep (Paper I)

Ocvirk, P., Pichon, C., Teyssier, R. 2008, MNRAS, 390,1326

Oppenheimer, B. D., Davé, R., Kereš, D., et al. 2010, MNRAS, 406, 2325

Petitjean, P., & Bergeron, J. 1990, A&A, 231, 309

Rao, S. M., & Turnshek, D. A. 2000, ApJS, 130, 1

Ribaudo, J., Lehner, N., Howk, J. C., et al. 2011, ApJ, 743, 207

Rigby, J. R., Charlton, J. C., & Churchill, C. W. 2002, ApJ, 565, 743

Rubin, K. H. R., Prochaska, J. X., Koo, D. C., & Phillips, A. C. 2011, arXiv:1110.0837

Rubin, K. H. R., Weiner, B. J., Koo, D. C., et al. 2010, ApJ, 719, 1503

Schneider, D. P., et al. 1993, ApJS, 87, 45

Simcoe, R. A., Sargent, W. L. W., Rauch, M., & Becker, G. 2006, ApJ, 637, 648

Steidel, C. C. 1995, QSO Absorption Lines, 139

Steidel, C. C., Dickinson, M., Meyer, D. M., Adelberger, K. L., & Sembach, K. R. 1997, ApJ, 480, 586

Steidel, C. C., Dickinson, M., & Persson, S. E. 1994, ApJ, 437, L75

Steidel, C. C., Erb, D. K., Shapley, A. E., et al. 2010, ApJ, 717, 289

Steidel, C. C., & Sargent, W. L. W. 1992, ApJS, 80, 1

Stewart, K. R., Kaufmann, T., Bullock, J. S., et al. 2011, ApJ, 738, 39

Tinker, J. L., & Chen, H.-W. 2008, ApJ, 679, 1218

Thom, C., Werk, J. K., Tumlinson, J., et al. 2011, ApJ, 736, 1

Tremonti, C. A., Moustakas, J., & Diamond-Stanic, A. M. 2007, ApJ, 663, L77

Tripp, T. M., & Bowen, D. V. 2005, IAU Colloq. 199: Probing Galaxies through Quasar Absorption Lines, 5

Tumlinson, J., Thom, C., Werk, J. K., et al. 2011, Science, 334, 948

van de Voort, F., Schaye, J., Booth, C. M., Haas, M. R., & Dalla Vecchia, C. 2011, MNRAS, 414, 2458

van de Voort, F., & Schaye, J. 2011, arXiv:1111.5039

Wang, W., & Wells, M. T. 2000, Statistica Sinicia, 10, 1199

Weiner, B. J., Coil, A. L., Prochaska, J. X., et al. 2009, ApJ, 692, 187

Weisheit, J. C. 1978, ApJ, 219, 829

Wolf, C., Meisenheimer, K., Rix, H.-W., et al. 2003, A&A, 401, 73

Wolynetz, M. S. 1979, Journal of the Royal Statistical Society, 28, 195

Yanny, B., & York, D. G. 1992, ApJ, 391, 569

Zibetti, S., Mènard, B., Nestor, D. B., Quider, A. M., Rao, S. M., & Turnshek, D. A. 2007, ApJ, 658, 161